UNIVERSIDAD NACIONAL MAYOR DE SAN MARCOS
COMITÉ ELECTORAL UNIVERSITARIO 2025

SOLICITUD DE INSCRIPCIÓN

ELECCIONES GENERALES 2025

FECHA : 12/04/2025

HORA : Hora 10 : Min. 55 : Seg.

TIPO DE POSTULACIÓN	**DECANO** X		
FACULTAD	CIENCIAS FISICAS		
DATOS DEL PERSONERO	ARÁMBULO MANRIQUE, MIGUEL ERNESTO		
	DNI 07418845	CELULAR	989004842
	correo electrónico: marambulom@unmsm.edu.pe		
DATOS DEL PERSONERO ALTERNO (FACULTATIVO)			
	DNI	CELULAR	
	correo electrónico:		
NOMBRE DEL CANDIDATO(A)	QUISPE GONZALES CÉSAR ALEJANDRO		

OBSERVACIONES

UNMSM
COMITE ELECTORAL
RECIBIDO
FECHA: 12/04 HORA: 10:55

NÚMERO DE FOLIOS	49

Firma del Personero

Cuarenta y nueve - 49

ELECCIÓN DE DECANOS DE LA UNIVERSIDAD NACIONAL MAYOR DE SAN MARCOS 2025

SOLICITUD DE INSCRIPCIÓN

(Formato 01)

Ciudad Universitaria, 10 de abril de 2025

Señor:
COMITÉ ELECTORAL UNIVERSITARIO
Universidad Nacional Mayor de San Marcos
Presente. -

Quien suscribe, **MIGUEL ERNESTO ARÁMBULO MANRIQUE, N° DNI 07418845, correo electrónico marambulom@unmsm.edu.pe, N° celular 989004842, dirección domiciliaria Calle Francisco de Toledo Mz. J, Lote 5, Urb. El Totoral, 2da Etapa, Santiago de Surco,** **PERSONERO GENERAL ACREDITADO**, solicita la inscripción del candidato al cargo de Decano de la Facultad de Ciencias Físicas de la Universidad Nacional Mayor de San Marcos.

Datos del candidato:

APELLIDOS Y NOMBRES	D.N.I. N°	GRADO DE ESPECIALIDAD	N° DE CELULAR	FIRMA DEL CANDIDATO	HUELLA DACTILAR (ÍNDICE DERECHO)
QUISPE GONZALES CÉSAR ALEJANDRO	10394420	DOCTOR	997938802		

El candidato firmante acredita al personero general como su representante y es la única persona autorizada para enviar y solicitar información al Comité Electoral Universitario.

Adjunto a la presente los siguientes documentos:

- **a.** Copia de DNI o carné de extranjería del candidato y del personero acreditado.
- **b.** Documento del grado de Maestro o Doctor (escaneo nítido).
- **c.** Declaración Jurada del candidato (**Formato 02**).
- **d.** Hoja de Vida del candidato (**Formato 03**).
- **e.** Plan de gobierno del candidato (**Formato 04).**

Expreso mi conformidad y compromiso de cumplimiento con las normas electorales.

DECLARO, conocer las consecuencias administrativas, civiles y penales por la falsedad de la información proporcionada, previstas en la Ley N°27444, en el Código Civil y Penal vigentes.

Atentamente,

Personero(a): **Miguel Ernesto Arámbulo Manrique**
CD N.º: **0A0140**
Doc. Identidad y Número: **DNI: 07418845**

HUELLA DACTILAR
(Índice Derecho)

Cuarenta y ocho - 48

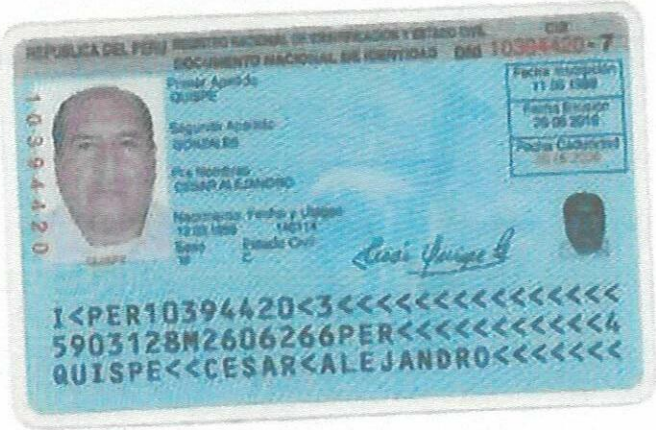

REPÚBLICA DEL PERÚ REGISTRO NACIONAL DE IDENTIFICACIÓN Y ESTADO CIVIL CUI
DUPLICADO DOCUMENTO NACIONAL DE IDENTIDAD DNI 07418845 - 7

0 7 4 1 8 8 4 5

ARAMBULO

Primer Apellido
ARAMBULO

Segundo Apellido
MANRIQUE

Pre Nombres
MIGUEL ERNESTO

Nacimiento: Fecha y Ubigeo
13 01 1963 140501

Sexo Estado Civil
M S

Fecha Inscripción 23 05 1997
Fecha Emisión 20 02 2023
Fecha Caducidad NO CADUCA

I<PER07418845<7<<<<<<<<<<<<<<<
6301134M0001018PER<<<<<<<<<<<6
ARAMBULO<<MIGUEL<ERNESTO<<<<<<

CONSTANCIA DE SUFRAGIO	CONSTANCIA DE SUFRAGIO	CONSTANCIA DE SUFRAGIO	CONSTANCIA DE SUFRAGIO

Índice Der.

Departamento
LIMA

Provincia
LIMA

Distrito
SANTIAGO DE SURCO

Dirección
CALLE FRANCISCO DE VALLEJO MZ.J LT.5 URB.EL TOTORAL II

Cuarto Nivel **140130**

Observaciones

Donación de Órganos NO

Grupo de Votación 202618

CARMEN VELARDE KOECHLIN
JEFE NACIONAL

000371 000350 90742W 0106 09618237

Cuarenta y seis - 46

UNIVERSIDAD NACIONAL MAYOR DE SAN MARCOS
Oficina General de Recursos Humanos
BOLETA DE PAGOS

PERSONAL DOCENTE PERMANENTE NORMAL **N°** PL20 BANCO Pago: 19/03/2025 Bolet 276 de 495
DEPENDENCI FACULTAD DE CIENCIAS FÍSICAS **MES:** MARZO **AÑO:** 2025

084492	10394420	QUISPE GONZALES, CESAR ALEJANDRO		Prin.T.C.40hr		01/12/1992
CODIGO	**DNI**	**APELLIDOS Y NOMBRES**		**CATEGORIA**	**CARGO**	**FECHA INGR.**
SPP	516191CQGSZ3	5903121QSGZC000	04071535091	0		UNMSM
REGIMEN	**CUSPP**	**AUTOGENERADO**	**CTA. ABONO BANCO**	**MESES**	**F. CESE**	**DECLARACION JURADA**

REMUNERACIONES

RM Docente Ordinario - Univ.	8,869.82

DESCUENTOS

Quinta Categoria	679.00
FFIPCOSAN-Fondo de	15.00

TOTAL	8,869.82
TOTAL DESCUENTOS:	694.00
TOTAL NETO:	8,175.82

Nota: Generado por la Oficina de Remuneraciones y Obligaciones Sociales, Telefono 619 7000, anexo 7608 Email: mesadepartes.oros@unmsm.edu.pe

Fecha de Envío: 3/21/25 10:43 AM
Correo Destino: cquispeg@unmsm.edu.pe

Quarenta y cinco - 45

UNIVERSIDAD NACIONAL MAYOR DE SAN MARCOS
Oficina General de Recursos Humanos
BOLETA DE PAGOS

PERSONAL	DOCENTE	PERMANENTE	NORMAL	**N°** PL20	BANCO	Pago: 19/03/2025		
						Bolet 276	de	495
DEPENDENCI	FACULTAD DE CIENCIAS FÍSICAS					**MES:** MARZO	**AÑO:**	2025

CODIGO	**DNI**	**APELLIDOS Y NOMBRES**		**CATEGORIA**		**CARGO**	**FECHA INGR.**
0A0140	07418845	ARAMBULO MANRIQUE, MIGUEL ERNESTO		Aux.TC.40hr			01/04/2001
REGIMEN	**CUSPP**	**AUTOGENERADO**	**CTA. ABONO BANCO**	**MESES**	**F. CESE**	**DECLARACION JURADA**	
SPP PRIMA	230221MAMMR4	6301131AMMRM000	04010572407	0		UNMSM	

REMUNERACIONES		**DESCUENTOS**	
RM Docente Ordinario - Univ.	5,233.00	AFP Prima	678.72
		Quinta Categoria	225.00

TOTAL	5,233.00
TOTAL DESCUENTOS:	903.72
TOTAL NETO:	4,329.28

Nota: Generado por la Oficina de Remuneraciones y Obligaciones Sociales, Telefono 619 7000, anexo 7608 Email: mesadepartes.oros@unmsm.edu.pe

Fecha de Envío: 3/21/25 10:43 AM
Correo Destino: marambulom@unmsm.edu.pe

República Federativa do Brasil

REPÚBLICA FEDERATIVA DO BRASIL
ORDEM E PROGRESSO

SP
PRO BRASILIA FIANT EXIMIA

unesp

Universidade Estadual Paulista "Júlio de Mesquita Filho"

Faculdade de Engenharia

Câmpus de Guaratinguetá

O Reitor da Universidade Estadual Paulista "Júlio de Mesquita Filho",
no uso de suas atribuições, confere a

César Alejandro Quispe Gonzáles

de nacionalidade peruana, natural do Peru, nascido a 12 de março de 1959,
portador da cédula de identidade RNE nº V540200-I,
o título de Doutor em Engenharia Mecânica,
Especialidade Aproveitamento de Energia,
obtido em 05 de julho de 2013, por ter concluído o Programa de Pós-graduação em Engenharia Mecânica,
outorgando-lhe o presente Diploma, para que possa usufruir de todos os direitos e prerrogativas legais.

Reitoria, 30 de outubro de 2013.

César Alejandro Quispe Gonzáles Diplomado	Prof. Dr. Marcelo dos Santos Pereira Diretor	Prof. Dr. Julio Cezar Durigan Reitor

Cuarenta y cuatro - 44

Cuarenta y tres - 43

Programa reconhecido pela Portaria Ministerial nº 1077, de 31/08/2012, publicada no D.O.U. de 03/09/2012, republicada em 13/09/2012.

O título conferido pelo presente Diploma foi homologado pela Congregação em 09/10/2013.

UNIVERSIDADE ESTADUAL PAULISTA
"JÚLIO DE MESQUITA FILHO"
SECRETARIA GERAL
GRUPO DE REGISTROS ACADÊMICOS

Diploma registrado sob n.º 33486
Processo nº 900/18/01/2013, de acordo com o disposto no artigo 48 da Lei 9394/1996.
São Paulo, 30/10/2013.

Raquel Schiavon Benatti
Responsável pelo GRA

De acordo.

Profa. Dra. Maria Dalva Silva Pagotto
Secretária Geral

Murilo Antunes de Oliveira - Tabelião
1º Tabelião de Notas e de Protesto de Letras e Títulos
Rua Pedro Marcondes, 7?, Centro - Guaratinguetá - SP - Fone: (12) 3133-3621 / 3622

RECONHEÇO, por semelhança sem valor econômico, a(s) firma(s) de: MARCELO DOS SANTOS PEREIRA. Dou fé.
Em test. da verdade.
Guaratinguetá - SP, 21 de novembro de 2013
R$ 4,25.
VERIDIANE DE CASSIA RIBEIRO VENORIO RODRIGUES
Segurança: 504949495048495149504948252

Válido Somente c/ Selo de Autenticidade

FIRMA 1
0357AA203615

CONSULADO GENERAL DEL PERÚ
Legalizada la firma de Veridiane de Cassia Ribeiro
quien desempena el cargo de not aut. del 1º notário
en São Paulo
N.º de Orden 4611
N.º de Tarifa 23
N.º de Actuacion 65
Derechos Percibidos: S/C
(SE LEGALIZA LA FIRMA Y NO EL CONTENIDO DEL DOCUMENTO)
San Pablo 16/04/2014

Fernando Alvarez Gamboa
Cónsul General Adscrito

CONSULADO ... São Paulo - Brasil

MINISTÉRIO DAS RELAÇÕES EXTERIORES
E R E S P
"Reconheço verdadeira por semelhança, a assinatura com o sinal MRE/ERESP A presente legalização não implica aceitação do teor do documento"
1 6 DEZ. 2013

- [ ] Ana Paula da Rocha Lima Bentes - Oficial de Chancelaria
- [ ] Gabriela Ferro Firmino Batista - Oficial de Chancelaria
- [ ] Mário Mauá Chaves Ferreira - Oficial de Chancelaria
- [x] Tatiana S. de Almeida - Oficial de Chancelaria

PERU
Nº: 001167
SECRETARIA GENERAL

ASAMBLEA NACIONAL DE RECTORES

Exonerado de revalida y reconocido por Resolución Nº 0835-2014-ANR 19-05 del 2014 de conformidad con el D.L. Nº 17662, D.S. Nº 028-69 E.D., D.L. Nº 1087, D.S. Nº 021-08-E.D., Resolución Ministerial Nº 035-2011-E.D., Reglamento General de la Comisión de Coordinación Interuniversitaria

Dr. RAÚL MARTÍN VIDAL CORONADO
Secretario General

R.E. ERESP

CERTIFICACIÓN DE FIRMAS

1. País / Country REPÚBLICA DEL PERÚ
   El presente documento público / This public document
2. ha sido firmado por / has been signed by **FERNANDO ALVAREZ GAMBOA**
3. quién actua en calidad de / acting in the capacity of **CÓNSUL GENERAL ADSCRITO**
4. y está revestido del sello / timbre de / bears the seal / stamp of **CONSULADO GENERAL DEL PERÚ EN SAO PAULO - BRASIL**

Certificado / Certified

5. en / at **SEDE CENTRAL - LIMA**
6. el / the **05/05/2014**
7. por / by MINISTERIO DE RELACIONES EXTERIORES
8. bajo el número / Nº **MRE1104840917051628982**
9. Sello/timbre / Seal/stamp
10. Firma / Signature

Zegarra Garcia Walter Rafael
Direccion General de Politica Consular
MINISTERIO DE RELACIONES EXTERIORES

Serie - 20 Nº 280314
www.rree.gob.pe

№ 020110

Cuarenta y dos - 42

ASAMBLEA NACIONAL DE RECTORES

Comisión de Coordinación Interuniversitaria

RESOLUCIÓN N° 0835-2014-ANR

Lima, 19 de mayo de 2014

EL PRESIDENTE DE LA ASAMBLEA NACIONAL DE RECTORES

*Vista la solicitud de don **CÉSAR ALEJANDRO QUISPE GONZÁLES,** quien pide la exoneración de exámenes de revalidación y el reconocimiento de su **título de Doctor en Ingeniería Mecánica, Especialidad de Aprovechamiento de Energía,** otorgado por la **Universidad Estatal Paulista "Júlio de Mesquita Filho" – REPÚBLICA FEDERATIVA DEL BRASIL;***

CONSIDERANDO:

Que el recurrente ha cumplido con presentar la documentación correspondiente y ha satisfecho los requisitos previstos en el Art. 2° del Decreto Supremo N° 028-69-ED;

Que el informe de la Asesoría Legal considera procedente el reconocimiento solicitado por haber satisfecho los requisitos formales de Ley;

Con el informe favorable de la Comisión de Reconocimiento y Certificación de Grados y Títulos de la Asamblea Nacional de Rectores;

De conformidad con los alcances del Decreto Ley N° 17662, Decreto Supremo N° 028-69-ED y la Ley Universitaria N° 23733;

En uso de las atribuciones que le compete a la Comisión de Coordinación Interuniversitaria en virtud del inciso o), del Artículo 13° del Reglamento General de la Comisión Interuniversitaria y de la Asamblea Nacional de Rectores;

SE RESUELVE:

*Reconocer el **título de Doctor en Ingeniería Mecánica, Especialidad de Aprovechamiento de Energía,** otorgado por la **Universidad Estatal Paulista "Júlio de Mesquita Filho" – REPÚBLICA FEDERATIVA DEL BRASIL,** a don **CÉSAR ALEJANDRO QUISPE GONZÁLES,** disponiéndose su inscripción en el Libro de Grados y Títulos de Reconocimiento de la Asamblea Nacional de Rectores.*

Regístrese y comuníquese.-

ASAMBLEA NACIONAL DE RECTORES – REPÚBLICA DEL PERÚ – PRESIDENTE

ORLANDO VELÁSQUEZ BENITES
Presidente

ASAMBLEA NACIONAL DE RECTORES – REPÚBLICA DEL PERÚ – SECRETARÍA EJECUTIVA

VÍCTOR RAÚL AGUILAR CALLO
Secretario Ejecutivo

ASAMBLEA NACIONAL DE RECTORES – REPÚBLICA DEL PERÚ – SECRETARIO GENERAL

RAÚL MARTÍN VIDAL CORONADO
Secretario General

/cgd

REPÚBLICA FEDERATIVA DO BRASIL

MINISTÉRIO DA CIÊNCIA E TECNOLOGIA

INSTITUTO NACIONAL DE PESQUISAS ESPACIAIS

O Diretor do Instituto Nacional de Pesquisas Espaciais, no uso de suas atribuições, confere a

César Alejandro Quispe Gonzáles

peruano, natural do Peru, nascido a 12 de março de 1959, portador da Cédula de Identidade nº RNE V540200-I – CGPI/DIREX/DPF, o título de

Mestre em Engenharia e Tecnologia Espaciais, Área de Concentração em Combustão e Propulsão

por haver cumprido em 05 de novembro de 2009 os requisitos necessários à obtenção do título. O presente Diploma outorga todos os direitos e prerrogativas estabelecidas pela legislação vigente.

São José dos Campos, 13 de abril de 2011.

Gilberto Câmara Neto
Diretor

César Quispe G.
Diplomado

Virginia Alves
Maria Virginia Alves
Chefe de Gabinete

José C. Becceneri
José Carlos Becceneri
Chefe do Serviço de Pós-Graduação

Cuarenta y uno - 41

Cuarenta – 40

MINISTÉRIO DA CIÊNCIA E TECNOLOGIA
INSTITUTO NACIONAL DE PESQUISAS ESPACIAIS

Curso reconhecido nos termos da Portaria MEC nº 524, de 29 de abril de 2008, publicada no D.O.U. de 30/04/2008.

José Carlos Becceneri
Chefe do Serviço de Pós-Graduação

2º TABELIÃO

UNICAMP
UNIVERSIDADE ESTADUAL DE CAMPINAS
Diretoria de Registro e Arquivo de Diplomas e Documentos

Diploma registrado sob n.º 511393
Proc. n.º 6342/11 nos termos do Art. 48 da Lei 9394/96.
Campinas, 18 / 10 / 2011

Luiz Fernando Gonçalves
Diretor de Serviço

Lêda Santos Ramos Fernandes
Secretária Geral

MINISTÉRIO DA CIÊNCIA E TECNOLOGIA
INSTITUTO NACIONAL DE PESQUISAS ESPACIAIS

Diploma registrado sob nº 1757 livro nº 01
fls. 50

São José dos Campos, 24 / 11 / 2011

Egídia I. Rosa Arantes
Assistente em Ciência e Tecnologia
Serviço de Pós-Graduação

2º TABEL

2ºTABELIÃO DE NOTAS - Dary Baptista dos Reis   Av.Eng.Fco Jose Longo,149 s17/9/12
Reconheço por semelhança (doc s/vr econ) as firmas de   (638606030689) 4
JOSE CARLOS BECCENERI, EGIDIA IGNACIO DA ROSA ARANTES
as quais conferem com os padrões registrados nesta serventia. Dou fé.
São José dos Campos, 2 de dezembro de 2011

Em testemunho da verdade

Valor: R$ 7,00   Ivone Piedade Gonçalves Guimarães Lopes - Escrevente
*** Válido somente com o selo de autenticidade

2º TABELIÃO DE NOTAS
Ivone Piedade Gonçalves Guimarães Lopes
TELEFONE 3921-60..
Av. Engº Fco. ... 149 - Lojas 7
CEP 12245-000 - São José dos Campos

Colégio Notarial do Brasil
FIRMA 2
1003AA037946

M.R.E. ERESP

PERU
Nº: 007010
SECRETARÍA GENERAL

ASAMBLEA NACIONAL DE RECTORES

Exonerado de reválida y reconocido por Resolución Nº 0361-2012-ANR 31/03 del 2012 de conformidad con el D.L. Nº 17662, DS. Nº 028-69 E.D. e Inc. o del Art. 13º del Reglamento General de la Comisión de Coordinación Interuniversitaria.

ANR
RAÚL MARTÍN VIDAL CORONADO
Secretario General

MINISTÉRIO DAS RELAÇÕES EXTERIORES
ERESP
"Reconheço verdadeira, por semelhança, a assinatura ... o sinal MRE/ERESP. A presente legalização não ... do documento."

16 DEZ. 2011

Ana Paula da Rocha Lima Bentes - Oficial de Chancelaria
Gabriela Ferro Firmino Batista - Oficial de Chancelaria
Mário Mauá Chaves Ferreira - Oficial de Chancelaria
Tatiana S. de Almeida - Oficial de Chancelaria

Treinta y nueve - 39

CONS. ... São Paulo

CONSULADO GENERAL DEL PERU
Legalizada la firma de
quien desempeña el cargo de
en
N.º de Orden 1531
N.º de Tarifa 23
N.º de Actuación 22
Derechos Percibidos: S/C.
(SE LEGALIZA LA FIRMA Y NO EL CONTENIDO DEL DOCUMENTO)
San Pablo 29 feb. 2012

REPÚBLICA DEL PERÚ
1 UN SOL 1
TIMBRE CONSULAR
UN SOL CONSULAR

CONSULADO GENERAL DO PERU
São Paulo

M. C. Eduardo Pérez del Solar
Cónsul General Adscrito

CERTIFICACIÓN DE FIRMAS

1. País / Country REPÚBLICA DEL PERÚ
   El presente documento público / This public document
2. ha sido firmado por / has been signed by **EDUARDO PEREZ DEL SOLAR**
3. quién actua en calidad de / acting in the capacity of **CÓNSUL GENERAL ADSCRITO**
4. y está revestido del sello / timbre de / bears the seal / stamp of **CONSULADO GENERAL DEL PERÚ EN SAO PAULO - BRASIL**

Certificado / Certified

5. en / at **SEDE CENTRAL - LIMA** 6. el / the **11/05/2012**
7. por / by MINISTERIO DE RELACIONES EXTERIORES
8. bajo el número / N° **MRE1397910943256755434**
9. Sello/timbre / Seal/stamp 10. Firma / Signature

MRE 355762

Aliaga Aliaga Segundo Saturnino
Dirección General de Política Consular
MINISTERIO DE RELACIONES EXTERIORES

Serie - 08 N° 456424

www.rree.gob.pe

REPUBLICA DEL PERU

ASAMBLEA NACIONAL DE RECTORES

Comisión de Coordinación Interuniversitaria

RESOLUCIÓN N° 0861-2012-ANR

Lima, 31 de julio de 2012

EL PRESIDENTE DE LA ASAMBLEA NACIONAL DE RECTORES

*Vista la solicitud de don **CÉSAR ALEJANDRO QUISPE GONZÁLES,** quién pide la exoneración de exámenes de revalidación y el reconocimiento de su **título de: Magister en Ingeniería y Tecnología Espaciales, Área de Concentración en Combustión y Propulsión,** otorgado por el **Instituto Nacional de Investigaciones Espaciales – REPÚBLICA FEDERATIVA DE BRASIL;***

CONSIDERANDO:

Asesoría Legal V°B° A.N.R.

Que, el recurrente ha cumplido con presentar la documentación correspondiente y ha satisfecho los requisitos previstos en el Art. 2° del Decreto Supremo N° 028-69-ED;

Que, el informe de la Asesoría Legal considera procedente el reconocimiento solicitado por haber satisfecho los requisitos formales de Ley;

Con el informe favorable de la Comisión de Reconocimiento y Certificación de Grados y Títulos de la Asamblea Nacional de Rectores;

De conformidad con los alcances del Decreto Ley N° 17662, Decreto Supremo N° 028-69-ED y la Ley Universitaria N° 23733;

En uso de las atribuciones que le competen a la Comisión de Coordinación Interuniversitaria en virtud del inciso o), del Artículo 13° del Reglamento General de la Comisión de Coordinación Interuniversitaria de la Asamblea Nacional de Rectores;

SE RESUELVE:

*Reconocer el **título de: Magister en Ingeniería y Tecnología Espaciales, Área de Concentración en Combustión y Propulsión,** otorgado por el **Instituto Nacional de Investigaciones Espaciales – REPÚBLICA FEDERATIVA DE BRASIL,** a don **CÉSAR ALEJANDRO QUISPE GONZÁLES,** disponiéndose su inscripción en el Libro de Grados y Títulos de Reconocimiento de la Asamblea Nacional de Rectores.*

Regístrese y comuníquese.-

ASAMBLEA NACIONAL DE RECTORES – PRESIDENTE

ORLANDO VELÁSQUEZ BENITES
Presidente

ASAMBLEA NACIONAL DE RECTORES – SECRETARIA EJECUTIVA

VICTOR RAÚL AGUILAR CALLO
Secretario Ejecutivo

ASAMBLEA NACIONAL DE RECTORES – SECRETARIO GENERAL

RAÚL MARTÍN VIDAL CORONADO
Secretario General

/jgv.

Treinta y siete-37

PERÚ | Superintendencia Nacional de Educación Superior Universitaria | Dirección de Registro y Reconocimiento de Grados y Títulos e Información Universitaria

REGISTRO NACIONAL DE GRADOS ACADÉMICOS Y TÍTULOS PROFESIONALES

Graduado	Grado o Título	Institución
QUISPE GONZALES, CESAR ALEJANDRO **DNI 10394420**	**TÍTULO DE DOCTOR EN INGENIERÍA MECÁNICA, ESPECIALIDAD DE APROVECHAMIENTO DE ENERGÍA** **Fecha de Diploma: 30/10/2013** *TIPO:* • ***RECONOCIMIENTO*** Fecha de Resolución de Reconocimiento: 19/05/2014 **Modalidad de estudios:** **Duración de estudios:**	UNIVERSIDAD ESTATAL PAULISTA "JULIO DE MESQUITA FILHO" ***BRASIL***
QUISPE GONZALES, CESAR ALEJANDRO **DNI 10394420**	**TÍTULO DE: MAGÍSTER EN INGENIERÍA Y TECNOLOGÍA ESPACIALES, ÁREA DE CONCENTRACIÓN EN COMBUSTIÓN Y PROPULSIÓN** **Fecha de Diploma: 13/04/2011** *TIPO:* • ***RECONOCIMIENTO*** Fecha de Resolución de Reconocimiento: 31/07/2012 **Modalidad de estudios:** **Duración de estudios:**	INSTITUTO NACIONAL DE INVESTIGACIONES ESPACIALES ***BRASIL***
QUISPE GONZALES, CESAR ALEJANDRO **DNI 10394420**	**TÍTULO DE INGENIERO MECÁNICO** **Fecha de Diploma: 27/06/1988** *TIPO:* • ***RECONOCIMIENTO*** Fecha de Resolución de Reconocimiento: 06/12/1989 **Modalidad de estudios:** **Duración de estudios:**	UNIVERSIDAD DE LA AMISTAD DE LOS PUEBLOS PATRICIO LUMUMBA ***URSS***

Treinta y seis - 36

UNIVERSIDAD NACIONAL MAYOR DE SAN MARCOS
COMITÉ ELECTORAL UNIVERSITARIO
2024 - 2025
RESOLUCIÓN RECTORAL N° 013410-2025-R/UNMSM

ELECCIÓN DE DECANO

CÉSAR ALEJANDRO QUISPE GONZALES

DECLARACIÓN JURADA
(Formato 02)

Ciudad Universitaria, 10 de abril del 2025

Yo, CÉSAR ALEJANDRO QUISPE GONZALES, identificado con DN1 10394420 y código docente N.º 084492, con grado académico de Doctor, miembro de la comunidad académica de la Universidad Nacional Mayor de San Marcos, como postulante al cargo de **DECANO** de la **Facultad de Ciencias Físicas**, declaro **BAJO JURAMENTO:**

a. Ser ciudadano en ejercicio
b. Ejercer docencia ordinaria en la categoría de docente principal en el Perú o en el extranjero, con no menos de tres (3) años en la categoría.
c. Tener una trayectoria académica y de investigación reconocida, con publicaciones en revistas indexadas o libros en su especialidad en un periodo no mayor de 7 años.
d. Tener experiencia en gestión pública.
e. No haber sido condenado por delito doloso con sentencia de autoridad de cosa juzgada.
f. No estar consignado en el registro nacional de sanciones de destitución y despido.
g. No estar consignado en el registro de deudores alimentarios morosos ni tener pendiente de pago una reparación civil impuesta por una condena ya cumplida.
h. No haber sido elegido decano en el periodo inmediato anterior.
i. No haber sido sancionado por hostigamiento o acoso sexual.

Asimismo, declaro conocer las consecuencias administrativas, civiles y penales por la falsedad de la información proporcionada, previstas en la Ley N° 27444, en el Código Civil y el Código Penal vigentes.

Atentamente,

César Quispe G.

Candidato(a): **César Alejandro Quispe Gonzales**
DNI 10394420

HUELLA DACTILAR
(Índice Derecho)

Treinta y cinco -35

QUISPE GONZALES CÉSAR ALEJANDRO

CANDIDATO A DECANO DE LA FACULTAD

0

HOJA DE VIDA
(Formato 03)

EXPERIENCIA EN GESTIÓN

Institución o empresa	Función	Periodo
Ministerio de Transporte	Ingeniero de Proyectos	2001 - 2007
CQG Ingeniería de Desarrollo EIRL	Gerente	2015 - 2023
UNMSM	Director de la EP de Ingeniería Mecánica de Fluidos	2017 - 2018
UNMSM	Director de la EP de Ingeniería Mecánica de Fluidos	2021 - 2022

PUBLICACIONES O INVESTIGACIONES

Tema	Medio de publicación y Fuente: URL	Año
Updated Review of Longshore Sediment Transport: Advantages, Disaventages and Comparisions Using a Satellite Image Methodology	doi: https://doi.org/10.3390/jmse12091660	2024
Simulación numérica para representación de corrientes inducidas por oleaje. Aplicación al puerto de Ilo – Perú	doi:10.15381/rif.v2711.27261 https://revistasinvestigacion.unmsm.edu.pe/index.php/fisica/article/view/27261/20975	2024
Comparison of the Thermal Efficiency of a Gas Turbine Working with Combustion and Detonation Chambers	doi://10.26678/ABCM.COBEM2021.COB2021-0929 https://abcm.org.br/proceedings/view/COB2021/0929	2021

CARGOS SURGIDOS DE UNA ELECCIÓN

Institución	Cargo	Periodo
UNMSM	Director de Departamento Académico de Ingeniería Mecánica de Fluidos	2019 - 2020
UNMSM	Miembro del Consejo de Facultad de Ciencias Físicas	2022 - 2024
		0

MEMBRESÍAS, PREMIOS Y RECONOCIMIENTOS

Membresías	Colegio de Ingenieros del Perú – N° 37728

Treinta y cuatro - 34

Premios	
Reconocimientos	

RELACIÓN DE PROCESOS ADMINISTRATIVOS Y/O JUDICIALES

Situación Actual	N° de casos
En proceso y sin sentencia por delito doloso	0
Con sentencia o sanción cumplida por delito doloso	0
En proceso o con sentencia por delito culposo	0

ESPECIALIDAD DE GRADO

Candidato(a): César Alejandro Quispe Gonzales
DNI 10394420

IMPRESIÓN DACTILAR
(Índice Derecho)

Institución	Año Inicio	Año Fin
Universidad de la Amistad de los Pueblos "Patricio Lumumba" – Mpsc+u - URSS	1982	1988
Instituto Nacional de Pesquisas Espaciais, Sao Paulo - Brasil	2008	2009
Universidad Estadual Paulista "Julio de Mesquita Filho" – Sao Paulo - Brasil	2009	2013

Treinta y tres - 33

ELECCIÓN DE DECANOS DE LA UNIVERSIDAD NACIONAL MAYOR DE SAN MARCOS 2025

(Formato 04)

PLAN DE GOBIERNO PARA EL PERIODO 2025 – 2029

Ciudad Universitaria, 10 de abril de 2025

El candidato **CÉSAR ALEJANDRO QUISPE GONZALES** presenta su plan de gobierno al Decanato de la ***Facultad de Ciencias Físicas*** de la Universidad Nacional Mayor de San Marcos:

Los ejes estratégicos de su Plan de Gobiernos son:

EJES ESTRATÉGICOS

Eje Estratégico 1	:	Formación académica con calidad para los estudiantes.
Eje Estratégico 2	:	Investigación e innovación en la comunidad académica.
Eje Estratégico 3	:	Extensión y proyección social universitaria para la sociedad.
Eje Estratégico 4	:	Modernización de la gestión institucional.
Eje Estratégico 5	:	Gestión del Riesgo de desastres y adaptación al cambio climático.

I. EJES ESTRATÉGICOS

EJE 1 Formación académica con calidad para los estudiantes.

OBJETIVOS	ACTIVIDADES	RESULTADOS
Implementación y desarrollo del modelo educativo de la UNMSM en la Facultad buscando asegurar los estándares de calidad	Actualización y mejora permanente de los planes curriculares en pre y posgrado	Programas curriculares actualizados conforme a las tendencias del mercado laboral y al avance del conocimiento científico y tecnológico
		Seguimiento del desarrollo de competencias para el mercado laboral, con el conocimiento académico apropiado
		Aseguramiento de la calidad académica contando con un plan curricular en permanente actualización e interdisciplinario
	Graduación y titulación	Incremento de la tasa de graduación y titulación de alumnos de pregrado y posgrado
	Modernización de laboratorios de enseñanza a través de proyectos de inversión	Laboratorios de enseñanza modernos, equipados con los últimos avances tecnológicos en actividades de ensayo y medición
Apoyar la internacionalización de la facultad y universidad mediante la movilidad estudiantil y docente	Intercambio académico de estudiantes para participar en programas de universidades extranjeras	Oportunidad de asistir a cursos de la carrera en otras universidades de su elección, incrementando la oferta académica.
		Acceso de estudiantes a nuevas tecnologías y sistemas educativos
	Apoyar la movilidad docente	Intercambio de experiencias y ensayos en procesos de enseñanza; así como mejorar los procesos de investigación e intercambio de experiencias buscando el desarrollo de ideas renovadoras

		Personal docente con conocimientos actualizados, ayudando al crecimiento profesional y académico del mismo
Impulsar el proceso de acreditación y de certificación	Promover la autoevaluación de la gestión pedagógica y administrativa	Mejora de la calidad del servicio educativo ofrecido y de los procesos internos y externos
	Impulsar la acreditación de las escuelas profesionales de Física e Ingeniería Mecánica de Fluidos	Mejora de la imagen institucional, al lograr el reconocimiento público de las carreras profesionales ofertadas

EJE 2 Investigación e innovación en la comunidad académica.

OBJETIVOS	ACTIVIDADES	RESULTADOS
Fomentar la cultura de investigación e innovación en la facultad	Promover la iniciación científica de estudiantes	Renovación y actualización de grupos de estudio estudiantiles para generar trabajos de investigación con miras a proseguir estudios de posgrado
		Generación de productos científicas, tecnológicos o de innovación, derivados del desarrollo de actividades de iniciación científica de los estudiantes de pregrado
		Creación de una revista para publicación de las tesis de titulación y productos de grupos de estudio estudiantiles
	Participación activa de docentes en actividades de investigación e innovación	Participación de todos los docentes en proyectos de investigación con y sin financiamiento
		Conseguir el apoyo y participación de la industria e instituciones privadas, que precisen de soluciones en sus actividades o procesos
Mejorar la calidad y el impacto de la investigación universitaria	Promover los congresos, talleres, seminarios, workshop nacionales e internacionales	Asistencia y participación de los estudiantes en congresos, talleres, seminarios y otros
		Desarrollo de patentes y productos de innovación
	Indexación de la Revista de Física en Scielo, Scopus y otros	Incremento en la cantidad y calidad de publicaciones científicas
		Reconocimiento y premiación de docentes investigadores

EJE 3 Extensión y proyección social universitaria para la sociedad.

OBJETIVOS	ACTIVIDADES	RESULTADOS
Promover la interacción e integración social contribuyendo en soluciones a las necesidades y desafíos de la sociedad	Colaboración con organizaciones comunitarias para su integración al sector productivo	Desarrollo e innovación de soluciones para abordar desafíos sociales
		Generación de oportunidades de comercio y emprendimientos
		Apoyo a la gestión de emprendimientos comunales
	Proyectos de servicio comunitario y voluntariado estudiantil	Desarrollo de habilidades personales y profesionales y fomento de la responsabilidad ciudadana
		Comprensión de problemas sociales actuales y toma de conciencia por parte de los estudiantes sobre la realidad social
Desarrollar actividades para contribuir al desarrollo de las comunidades impulsando el desarrollo	Promover las actividades multidisciplinarias, en base a las líneas de proyección social de la facultad	Elaboración de proyectos de desarrollo en áreas de competencia y saber de las escuelas de la facultad

cultural, transferencia del conocimiento y tecnología, hacia sectores sociales de la comunidad	Ejecución de actividades de capacitación y educación continua, considerando las políticas de extensión universitaria de la facultad	Mejora del nivel de conocimiento y cultural de las poblaciones de las comunidades vinculadas.
		Impacto en la mejora de la calidad de vida de los pobladores de comunidades beneficiadas.
Mejorar la imagen y reputación de la universidad en la sociedad	Colaboración con las organizaciones y otros entes comunitarios	Mejora y fortalecimiento de la relación sociedad - universidad
		Mayor presencia de la universidad y reconocimiento de la sociedad

EJE 4 Modernización de la gestión institucional

OBJETIVOS	ACTIVIDADES	RESULTADOS
Alcanzar una gestión eficiente de la facultad	Mejora continua de los procesos administrativos	Identificación de problemas y mejora en la capacidad de resolución de ellos
		Mejora en el índice de satisfacción de docentes, administrativos y estudiantes
	Mejora de los canales de comunicación sobre las actividades en la facultad	Mantener informados a los integrantes de la facultad aprovechando las diferentes tecnologías de información
		Transparencia en los temas tratados y acuerdos tomados en Consejo de Facultad y decanato
	Mejora y gestión del talento humano	Integración y capacitación del personal
		Transparencia y respeto a la dignidad docente, en procesos de ratificación y promoción docente, disminuyendo el numero de casos en apelación
		Mejorar la motivación para una mejor atención de los usuarios
	Mejora continua de los procesos financieros y contables	Transparencia en la información de ingresos y egresos de la facultad
		Transparencia en la gestión económica de la facultad y uso eficiente de los recursos
		Cumplimiento de los planes anuales de inversión y mantenimiento
Integrar las tecnologías de información en apoyo de la gestión de la facultad	Capacitación en competencias y herramientas digitales	Mejora de la productividad del trabajo y atención en la facultad
		Logro de metas fijadas en la facultad

EJE 5 Gestión del Riesgo de Desastres y adaptación al cambio climático.

OBJETIVOS	ACTIVIDADES	RESULTADOS
Fomentar la cultura de protección civil	Difusión de programas y materiales de prevención de desastres	Mejora de la conciencia sobre riesgos y peligros ocasionados por los desastres naturales
		Conocimiento de políticas de preparación, mitigación y respuestas frente a desastres naturales
	Realización de cursos de capacitación para docentes, administrativos y estudiantes en materia de protección civil	Conocimiento de reglas y recomendaciones de comportamiento frente a los desastres naturales
		Mejora de los valores de solidaridad frente a los desastres naturales
Reducir la vulnerabilidad frente a los desastres naturales	Identificación y evaluación de riesgos posibles por desastres naturales	Identificación de lugares seguros
		Establecer medidas y acciones que con lleven a la reducción de la vulnerabilidad
	Mejora del plan de gestión de riesgo frente a desastres naturales y adaptación al cambio climático	Mejoramiento de la capacidad de respuesta frente a desastres naturales e impactos del cambio climático

Limitar impactos y reducir vulnerabilidades frente al cambio climático	Reducción y control de actividades que generen gases de efecto invernadero	Menores impactos en la salud y confort del personal de la facultad
Mejorar la resiliencia del sistema humano frente al cambio climático	Gestión integral de riesgos y políticas sostenibles y adaptación al clima	Mejora de la capacidad de respuesta ante los impactos del cambio climático

Candidato(a): **César Alejandro Quispe Gonzales**

Doc. Identidad y Número: 10394420

IMPRESIÓN DACTILAR

(Índice Derecho)

Constancia de Registro de Publicaciones Científicas

El Vicerrector de Investigación y Posgrado de la Universidad Nacional Mayor de San Marcos hace constar que:

El profesor(a): **CESAR ALEJANDRO QUISPE GONZALES**
de la Facultad de: **Ciencias Físicas**
ha registrado las siguientes publicaciones:

Nro Publicaciones:	32
Puntaje Total:	52.50

Artículos Publicados en Revistas de Investigación

Art. Primario en Revista Indexada

Año	Título	Publicación	ISSN	Obs
2014	Ecological efficiency in glycerol combustion	Applied Thermal Engineering	1359-4311	
2013	Glycerol: Production, consumption, prices, characterization and new trends in combustion	Renewable and Sustainable Energy Reviews	1364-0321	
2011	Estudio teórico de la onda de combustión: Caso de la onda generada en la combustión del metano y aire	Revista de Investigación de Física	1605-7724	

Art. Primario en Revista No Indexada

Año	Título	Publicación	ISSN	Obs
2014	Diseño aerodinámico de un túnel de viento de bajas velocidades	Revista de Investigación de Física	1605-7724	
2012	Análisis de flujo y su influencia en el diámetro medio de las gotas para inyectores de mistura interna tipo Y	Revista de Investigación de Física	1605-7724	
2012	Comparación de costos de producción conjunta de electricidad y calor usando gas natural y glicerol	Revista de Investigación de Física	1605-7724	
2011	Estudio teórico de la onda de combustión: Caso de la onda generada en la combustión del metano y aire	Revista de Investigación de Física	1605-7724	
2009	Desgaste en los sistemas de inyección diesel por efecto del elevado contenido de azufre en el petróleo diesel 2	Revista de Investigación de Física	1605-7724	

Revista no ISI

.ño	Título	Publicación	ISSN	Obs
2007	Briquetas de residuos sólidos orgánicos como fuente de energía calorífica en cocinas no convencionales	Revista de Investigación de Física	1605-7724	
1999	Cavitación y altura de succión permisible de la turbina	Hidráulica & Termofluídos		

Resúmenes de Eventos Científicos

Art en Extenso en Evento Internacional

Año	Título	Libro	Ciudad	Obs
2012	Análisis de flujo y su influencia en el diámetro medio de gotas para inyectores de mistura interna tipo Y	Memoria Técnica Resúmenes VII Congreso Bolivariano de Ingeniería Mecánica	Cusco	
2012	Comparación de costos de producción conjunta de electricidad y calor, usando gas natural y glicerol	Memoria Técnica Resúmenes VII Congreso Bolivariano de Ingeniería Mecánica	Cusco	
2011	Análise do Escoamento em Regime Subsônico e Influência no	Actas do X Congreso	Oporto	

2011	Costos de producción de vapor y electricidad en un ciclo de cogeneración: turbina a gas - caldera de recuperación - turbina a vapor	Proceedings and Book of Abstracts of 9th Latin-American congress on electricity Generation and Transmission	Mar del Plata	
2010	Propagation of combustion waves in Van der Waals gases	Proceedings of ENCIT 2010	Uberlandia	
2009	Propagation of combustion waves in Noble-Abel gases	Proceedings of COBEM 2009	Gramado	

Art en Extenso en Evento Nacional

Año	Título	Libro	Ciudad	Obs
2011	Reactor anaerobio para la producción de biogás aprovechando las aguas del colector de la Taboada - Callao		Lima	

Congreso Nacional

Año	Título	Libro	Ciudad	Obs
1996	Teoría básica de bombas	Trabajos del Seminario "Bombas, Diseño, Construcción, Selección, Instalación, Mantenimiento y Reparación"	Lima	
1993	Hidrodinámica electromagnética: presente y futuro	Resúmenes del I Simposio Nacional de Mecánica de Flúidos y Tecnología Conexa	Lima	

En extenso - Internacional

Año	Título	Libro	Ciudad	Obs
2021	Comparison of the thermal efficiency of a gas turbine working with combustion and detonation chambers	Proceedings 26th International Congress of mechanical Engineering	Congreso Virtual	
2020	Establecimiento de una red limnimetrica en las hidrovías de la Amazonia peruana	Atas das 6ta Jornadas de Engenharia Hidrográfica /1as Jornadas Luso-Espanholas de Hidrografia	Lisboa	

En extenso - Nacional

Año	Título	Libro	Ciudad	Obs
2023	Aprovechamiento de la energía turbulenta para la optimización del enfriamiento de piezas de fundición, mediante la aplicación de un mezclador hidráulico por inducción hidrodinámica	Programa general XXV CONIMERA 2023	LIMA	

Tesis asesoria

Asesor - Título profesional

Año	Título	Universidad	País	Obs
2022	Análisis del sistema de despacho de gasohol con mezcla en línea, bajo el concepto de transferencia de custodia		Perú	
2019	Cálculo de un sistema contraincendio para una planta de generación de energía en la industria láctea		Perú	
2019	Cálculo hidráulico del sistema de relaves – caso Mina Invicta		Perú	
2019	Cálculo y selección de equipos de un sistema de aire acodicionado para salas blancas en instalaciones hospitalarias		Perú	

	aducción de la C.H de Chaglla	
2018	Determinación del coeficiente de conductividad térmica del concreto con aditivo de poliuretano residual	Perú
2017	Análisis térmico y selección de ciclo de proceso para la implementación de una planta piloto de 10mw de energía geotermal en el campo geotérmico de Calientes - Tacna	Perú
2013	Caracterización, evaluación de la confiabilidad y mejoras técnicas de un sistema eólico de baja potencia con generador de imanes permanentes - aerogenerador de 100W	Perú

Tesis de Pre y Postgrado

Tesis de Maestría

Año	Título	Universidad	País	Obs
2009	Propagação de ondas de combustão em gases de Noble Abel e de van der Waals		BR	

Tesis Doctoral

..io	Título	Universidad	País	Obs
2013	Investigação de injetores tipo y e efervescentes para a atomizacão da mistura de glicerina e etanol		BR	

Se expide la presente constancia a solicitud del interesado(a)

Lima, 09 de septiembre de 2024

UNMSM Firmado digitalmente por NIÑO MONTERO Jose Segundo FAU 20148092282 hard
Motivo: Soy el autor del documento
Fecha: 09.09.2024 09:35:16 -05:00

Dr. José Segundo Niño Montero
Vicerrector

Constancia de Grupos de Investigación de la Universidad Nacional Mayor de San Marcos

El Vicerrector de Investigación y Posgrado hace constar que:

CESAR ALEJANDRO QUISPE GONZALES, docente permanente de la Facultad de Ciencias Físicas ha registrado participación en el(los) siguiente(s) Grupo(s) de Investigación:

Nombre corto GI	Nombre de Grupo	Condición	Resolución Rectoral	Fecha de creación GI
MECFLUET	MECÁNICA DE FLUIDOS - ENERGÉTICA Y TERMOFLUIDOS	Coordinador	01199-R-19	08/08/2017

Se expide la presente constancia a solicitud del(de la) interesado(a) para los fines que considere conveniente.

Lima, 09 de septiembre de 2024

UNMSM
Firmado digitalmente por NIÑO MONTERO Jose Segundo FAU 20148092282 hard
Motivo: Soy el autor del documento
Fecha: 09.09.2024 09:35:38 -05:00

Dr. José Segundo Niño Montero
Vicerrector

Journal of
Marine Science and Engineering

MDPI

Review

Updated Review of Longshore Sediment Transport: Advantages, Disadvantages, and Comparisons Using a Satellite Image Methodology

César M. Alpaca-Chacón [1,2,*], Bismarck Jigena-Antelo [1,*], César A. Quispe-Gonzales [2], Douglas D. Sarango-Julca [2], Antonio Contreras-de-Villar [3] and Juan J. Muñoz-Perez [1]

1 CASEM (Andalusian Higher Marine Studies Center), University of Cadiz, 11510 Puerto Real, Spain; juanjose.munoz@uca.es
2 Professional School of Fluid Mechanics Engineering, Universidad Nacional Mayor de San Marcos, Lima 15001, Peru; cquispeg@unmsm.edu.pe (C.A.Q.-G.); dsarangoj@unmsm.edu.pe (D.D.S.-J.)
3 ETSIA (Algeciras Higher Technical School of Engineering), University of Cadiz, Avda. Ramón Puyol s/n, 11202 Algeciras, Spain; antonio.contreras@uca.es
* Correspondence: cesar.alpacachacon@alum.uca.es (C.M.A.-C.); bismarck.jigena@gm.uca.es (B.J.-A.)

Abstract: This review updates the different categories and formulations of the calculation of longshore sediment transport (LST) and summarizes their advantages and disadvantages. Most of these methodologies require calibration for areas different from those studied by their authors. Thus, a method of validation and calibration is presented here by processing satellite images with CoastSat software (release v 2.7) to determine accretion and erosion volumes. This low-cost methodology was applied to Salaverry Beach (Peru) to compare the results of the different formulations. A range of variation between −96% and +68% was observed concerning the error, with van Rijn's formula being the most accurate for this particular case.

Keywords: erosion; accretion; CERC; low-cost methodology; Salaverry Beach; Perú

check for updates

Citation: Alpaca-Chacón, C.M.; Jigena-Antelo, B.; Quispe-Gonzales, C.A.; Sarango-Julca, D.D.; Contreras-de-Villar, A.; Muñoz-Perez, J.J. Updated Review of Longshore Sediment Transport: Advantages, Disadvantages, and Comparisons Using a Satellite Image Methodology. *J. Mar. Sci. Eng.* **2024**, *12*, 1660. https://doi.org/10.3390/jmse12091660

Academic Editor: Francesca De Serio

Received: 5 August 2024
Revised: 7 September 2024
Accepted: 12 September 2024
Published: 16 September 2024

1. Introduction

One of the most frequently needed variables in coastal engineering is the total longshore sediment transport (LST) rate. This is essential for addressing issues related to filling dredged channels, spreading beach fills, disposing of dredged material, and the morphodynamic reaction of coastal areas for engineering projects. In order to obtain adequate management of coastal engineering for port design or beach maintenance applications with the inclusion of structures such as breakwaters and others, it is imperative to have a solid knowledge of LST.

There are currently different methods for dealing with the issue of LST. In LST studies, energy, current power, and dimensional analysis methods are used, as they are simple and easy to calculate, as opposed to computational numerical models, which are more complex and require greater computational expenditure. When it comes to energy methods, we have two subclassifications. While the current energy-method approach is more broadly applicable to any sediment transport circumstance, the energy-flux method was specifically developed for coastal sediment transport. The method of balancing forces is more related to the shear stresses on the seabed, and the dimensional analysis method employs a set of dimensionless parameters for the study of LST [1].

Recent improvements in numerical simulations depicting coupled physical systems have demonstrated that the interaction of currents, waves, and winds can have a significant impact on nearshore processes [2–4].

These investigations all demonstrate how strongly waves and currents interact. A correct explanation of coastal hydrodynamics requires an understanding of both waves and

Venticinco-25

tidal processes. Currents and tides are observed to affect wave breaking and sea turbulence, according to Ardhuin et al. [4].

The three primary categories of the LST prediction technique are energy methods, which are further divided into energy-flux approaches and the current energy method, dimensional analysis, and balancing forces.

A brief summary of the state of the art should begin with USACE [5], Tomasicchio et al. [6], and Swart [7], who introduced mean grain size as a variable of LST in sands. On the other hand, Nichols and Wright [8] and Chadwick [9] studied coarser sediments, combining data from sedimentation traps and electronic and aluminum tracers. Moreover, Chadwick [9] and Brampton and Motika [10] obtained other coefficients for dimensionless calibration parameters.

Later, by using the H_s (significant wave height, in meters) for the 46 data points that most closely matched their selection criteria for $D_{50} < 1$ mm, Schoonees and Theron [11,12] fitted an energy-flux expression. The coefficient of determination (R^2) for $D_{50} > 1$ mm was significantly poor.

As for the energy-flux method, the CERC equation [5] (created by the Corps of Engineers, US Army) is available. It was developed for sandy beaches and is widely used around the world to this day. There are also the formulas of Inman and Bagnold [13], Komar [14]. Several authors have proposed values for the calibration constant K, including Greer and Madsen [15], Watts [16], and Caldwell [17], which were of little use.

Regarding the current power method, Bailard [18] and Bagnold [19,20] propose an LST equation derived from a locally time-averaged equation. Bailard [18] derived a K value for CERC by integrating the LST rate averaged over local time, used in conjunction with H_{rms} (root-mean-square wave height, in meters). He introduced the median diameter variable D_{50} through the velocity of particle fall. Bagnold [19,20] indicated that a percentage of the current is reversed in suspended and background LST.

The LST method of balancing forces is connected to the bed's shear stresses, derived from the currents induced by the waves, and, therefore, is an evolution towards energetic methods and dimensional analysis. Frijlink [21] proposed the first such formula, divided into two parts: one for the calculation of currents and the other for LST. Bijker [22,23] used hydrodynamic methods averaged by their integration into the wave zone. Damgaard and Soulsby [24] also used this method based on a formula created by Soulsby [25], in which the authors used simplifications, such as a uniform beach, waves in shallow water, constant breakage, and no refraction, among others.

The dimensional analysis method was developed thanks to laboratory experiences, calibrated with oceanographic parameters, and corroborated with LST rates. Its expressions are very similar to those of the energy-flux method. Evidently, like any dimensionless method, it was proposed based on dimensionless physical parameters. van Hijum and Pilarczyk's formula [26] was derived from their laboratory experiments and those from van Hijum [27]. The LST formula by Kamphuis et al. [28] was created with consideration for beach slope and grain size, specifically for usage on sandy beaches. This came about as a result of numerous lab experiments and an extensive collection of field data. Kamphuis refined this formula himself [29] by using an additional set of hydraulic model tests.

In addition, van der Meer [30] proposed an alternative LST equation for the dimensional analysis method, modifying the threshold parameters and the calibration constant. This equation is also valid for coarse-grained beaches, given its comparison with experimental data from van Hijum and Pilarczyk [26], who concluded that gravel beaches absorb more energy from percolation when compared to Schoonees and Theron sandy beaches [31].

According to van Wellen [1], equations based on energy methods give good results for coarse-grained beaches, whereas dimensional analysis equations overpredict LST results. Thus, it should be noted that the former models do not give the same results, as they cannot be calibrated for all wave conditions and beach types. For example, in LST studies on pebble beaches, calibration is mainly performed using results from the use of traps or shoreline profilers (all of them high cost) [1]. On the other hand, tracers are the best technique for calibrating LST models, according to Muñoz-Perez et al. [32], rather than expensive traps. However, the results of the LST calculation will remain uncertain and require further validation [33].

For all these reasons, and after numerous investigations and the collection of field and laboratory data, a general formula has not yet been found for all types of beaches and all places because of the different geographical and environmental conditions of the littoral and the ocean.

Due to being faced with this reality, this paper aims to present an update of the different LST formulas created to date. In addition, their advantages and disadvantages are highlighted, and an estimate of the error percentage by applying the different formulations to a particular case is found. As a reference value, an easy and low-cost method is proposed, namely the calculation of the erosion/accretion volume by comparing satellite photos.

Study Site

The geographical coordinates of the study area (the port of Salaverry in Peru) are −8.1650139° S and −79.0108019° W (Figure 1). Swell waves come from the SW direction (85% probability) and, to a lesser degree, from the S and SSW directions. The mean annual breaking wave height is H_b = 2.23, while the significant wave height of the swell is H_s = 2.1 m. Its peak period (T_p) is 14.21 sec, and its predominant deepwater direction is 213.5°. The sediments are mostly very fine sand D_{50} = 0.16 mm. The tidal range on average is 0.80 m, and the tidal range in syzygies is 1.28 m. The LST calculation will be carried out using the CoastSat method as validation for the Port of Salaverry (Peru). The data were obtained from private studies by the company H&O Ingenieros S.A., the National Port Company (ENAPU), and the Directorate of Hydrography and Navigation of the Peruvian Navy (DHN).

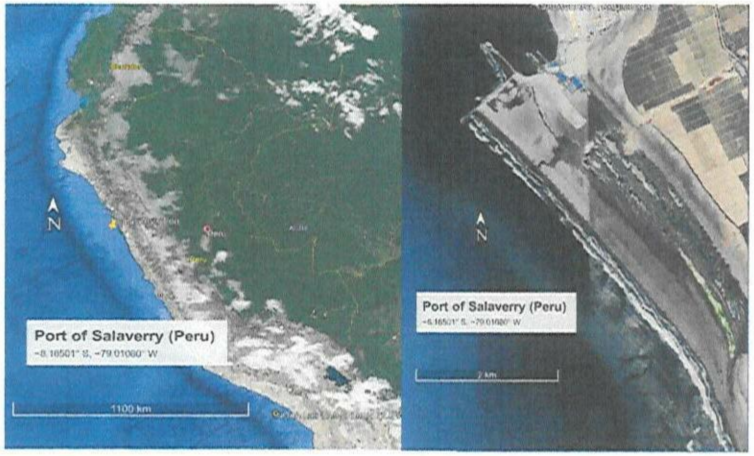

Figure 1. Port of Salaverry (Perú). Fuente: Google Earth Pro (2024).

Hydrodynamic forcing used (wave parameter, water depth, and D_{50}) in situ data. Numerical models were not used for current velocity prediction, as they are not necessary for the LST calculations. Hydrodynamic variables are included as constant values in the LST calculations.

2. LST Formulations

In order to compile the different formulas developed over the years for the calculation of sediment transport, it was decided to group them into three categories according to the criteria contemplated for their conception and elaboration. The first group is based on energy methods and the second group on the balance of forces. The third group of equations is based on dimensional analysis.

2.1. *Energy Methods*

The methods based on energy are subdivided into energy flux and current energy approaches. While the current energy approach is more broadly applicable to any sediment transport condition, such as LST in rivers (estuaries), the energy-flux method was especially established for LST [2].

2.1.1. Energy-Flux Method

Waves travel from the deep ocean to the coast and dissipate their energy in different ways, including the resuspension of sedimentary material and the net movement of water masses in the form of currents (transverse and longitudinal). The angle of incidence of the wave fronts and their energy gradient along the coast determine a parallel net mass flow, which forms a longitudinal current (Figure 2). This component is mainly responsible for the morphological alterations of beaches and the transport of sediments [34].

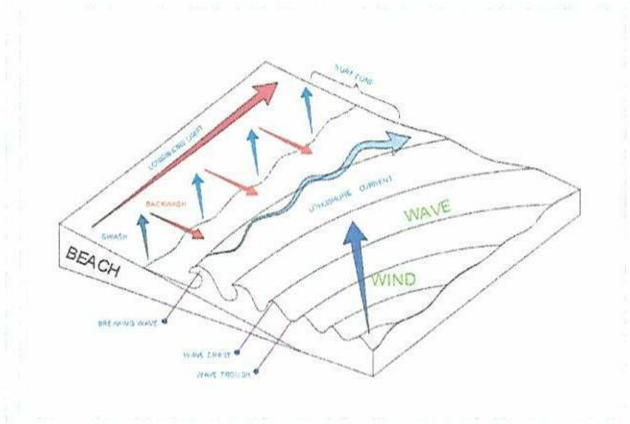

Figure 2. Sketch showing LST based on wind direction and coastal waves.

According to Komar and Inman [35], the foundation of the LST energy-flux approach is based on the fact that wave power, P (W/m), is proportional to the submerged sediment transport rate, I (kg/s). The CERC (Coastal Engineering Research Center) equation, which was put forth by the USACE (US Army Corps of Engineers), is the most well-known formula for this category [5]. The formula includes background and suspended LST, expressed as the following:

$$I = K \cdot P \tag{1}$$

where K is a coefficient that was determined empirically. Through the use of the root-mean-square wave height in the breaking (b) zone, the K value used for $H_{b,rms}$ (root-mean-square breaking wave height, in meters) is 0.77 [15]. By using significant wave height, H_s, instead

Veinticuatro-24

of H_{rms}, a few more datasets were added to the CERC [5] equation, updating the value to $K = 0.39$. However, $K = 0.92$ is the comparable result using $H_{b,rms}$, according to Rosati et al. [36].

$$P = (E \cdot C_g)_b \cdot \sin\theta_b \cdot \cos\theta_b \tag{2}$$

Here, $E = \frac{1}{8} \cdot \rho \cdot g \cdot H_b^2$ is the energy density of waves (in J/m^2), ρ is the density of seawater (in kg/m^3), gravity accelerates at an average speed of $g = 9.81\ m/s^2$, the wave's height in the breaking zone is expressed in meters (or H_b), and θ_b is the wave's angle at the breaking zone (the distance between the wave's crest line and the coastline). Finally, C_g is the velocity of the group celerity (m/s), given by

$$C_g = \frac{c}{2} \cdot \left(1 + \frac{2kh}{\sinh 2kh}\right) \tag{3}$$

where c is the velocity of the wave, the wave number is k (m^{-1}), depth is represented by h (m), and the volumetric LST (Q in m^3/s) is

$$Q = \frac{I}{\Gamma} = \frac{K \cdot P}{\Gamma} \tag{4}$$

with

$$\Gamma = \frac{(\rho_s - \rho) \cdot g}{1 + e} \tag{5}$$

ρ_s is the sediment's density (2650 kg/m^3 approx.), e is the void ratio (0.6 approx.), and Γ is the ratio used to convert volumetric transport rates from mass ones.

Equation (4) gave acceptable results with the calibrated K applied to the break zone. The calibrated K was lower than the theoretically used version and has a strong influence on transport velocity in the breaker zone [37].

Swart [7] introduced the variable D_{50} within K for medium-sized sediments.

$$Q = 0.116\, log_{10}\left(\frac{0.0146}{D_{50}}\right) \cdot \frac{P}{\Gamma} \tag{6}$$

Chadwick [9] included two dimensionless parameters, D_{90}/H and L/D_{90}, in the CERC equation, where the wavelength is represented by L (m). H is the representative height of the waves (m).

$$Q = \frac{K \cdot P}{\Gamma} \left(\frac{L}{D_{90}}\right)^{\varepsilon_1} \left[1 - \frac{8.1\, D_{90}}{H}\right]^{\varepsilon_2} \tag{7}$$

In this Equation, it is necessary to know the ε_1 and ε_2 for each location. Chadwick [9] used Equation (7), making $\varepsilon_1 = 0$ and $\varepsilon_2 = 1$, resulting in

$$Q = \frac{K \cdot P}{\Gamma} \left[1 - \frac{8.1\, D_{90}}{H}\right] \tag{8}$$

When Chadwick [9] applied Equation (8) compared to the normal CERC equation (4) that is, without the threshold and particle size terms of Equation (7), the K value produced was 7%. However, applying the extended field for data, Shoreham data in Bray et al. [38] resulted in $K = 0.07$ (measuring wave height with H_{rms}), which was only 9% of the original K value.

Chadwick [9] adapted the information from van Hijum [27] and van Hijum and Pilarczyk [26] in terms of the breaking wave condition.

$$Q = 0.0013 \left(g\, D_{90}^2\, T_s\right) \cdot w \cdot (w - 8.3) \cdot \sin\theta_b \tag{9}$$

$$w = \frac{H_{ob}\, \sqrt{\cos\theta_b}}{D_{90}} \tag{10}$$

Here, T_s is the significant wave period in s, H_{ob} is the significant wave height in wave breaking in m, and θ_b is the wave angle in wave breaking (Figure 3).

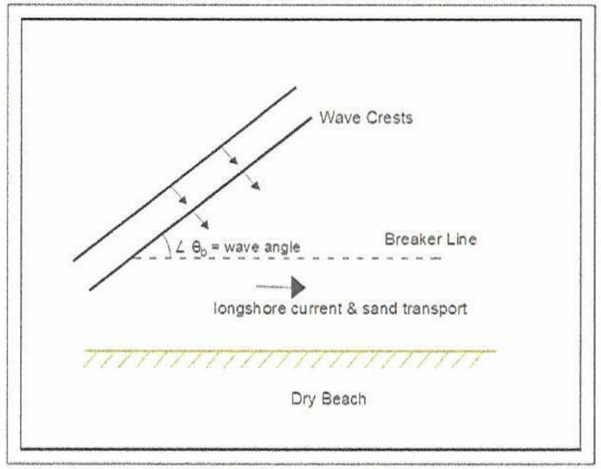

Figure 3. Wave angle in wave breaking in LST.

Subsequently, Schoonees and Theron [11,12] found a correlation for $D_{50} < 1$ mm and $K = 0.41$ by using a correlation value of $R^2 = 0.77$.

$$I = 0.41\, P\, \left(R^2 = 0.77\right) \tag{11}$$

Tomasicchio et al. [39] proposed a general longshore transport (GLT) procedure that belongs to the typology based on an energy-flux approach and is combined with an empirical relationship between wave-induced forcing and the number of moving beach sediment units. To be more precise, the GLT approach takes a suitable mobility index into account and assumes that the material (unit) moves with the same obliquity of breaking and reflected waves at the breaker depth during both up- and down-rush. If, and only if, a unit is removed from an updrift area of an extension equal to the longitudinal component of the displacement length, $l_d \sin\vartheta_d$, where l_d is the displacement length, and ϑ_d is its obliquity, then the unit passes through a particular control section. This methodology will not be expanded during this review due to the extension of the calculations; we are thinking about developing a fascinating approach in a subsequent article.

2.1.2. Current Energy Method

Water flows from coastal systems are accompanied by sediment transport, which requires the work of energy of waves and wind (effort at the bottom). The potential energy of the water (due to its elevation) is transformed into kinetic energy, which it uses to move the sediment. Another part dissipates to overcome the friction at the boundaries and in the bed. The rate of potential energy expenditure over time is the power of the current, a fundamental parameter for the evolution of a coastal system.

Bagnold [19] pointed out that a percentage of the wave power produces suspended and background LST, as the energy of the current is able to transport deposit particles in the current's direction.

Veimtitrés-23

Based on Bagnold [20], Bailard [18] presented an equation for LST averaged over local time, which applies to the K from the CERC formula for H_{rms}.

$$K = \varepsilon_b K_1 + \varepsilon_s K_2 + \varepsilon_s^2 K_3 \tag{12}$$

Equation (12) considers the load at the bottom, as well as the suspended load. Additionally, he notes that on coarse-grained beaches, suspended sediment transfer is unlikely to happen because the LST can be overestimated.

Bailard [18] proposed $\varepsilon_b = 0.13$ and $\varepsilon_s = 0.32$. The K_1, K_2, and K_3 values, which are consistent with eight field and two USACE laboratory datasets [5], are given by the following relationships:

$$K_1 = 0.385 + 20\sin^2(2\theta_b);\ K_2 = 0.228\ {}^{u_{mb}}/_{w_s};\ K_3 = 0.123 tan\beta\left(\frac{u_{mb}}{W_s}\right)$$

The last term in Equation (12) represents the suspended load, and the first term can be neglected because its input to the formula is small. Bailard [18] concluded that the modification of the coefficient K allows us to broaden the CERC equation's use when considering the velocity of fall, w_s, for representative grains.

With these considerations, the K value is obtained from

$$K = 0.05 + 0.007\ {}^{u_{mb}}/_{w_s} + 2.6\sin^2(2\theta_b) \tag{13}$$

where u_{mb} is the maximum orbital speed below the surface of the sea (m/s), w_s is the speed at which sediment falls (m/s), and $tan\beta$ is the average beach slope. The original meaning of u_{mb} is the maximum orbital speed on the bottom, though the maximum orbital speed below the surface equals the maximum orbital velocity on the bottom because Bailard [18] used the shallow water wave theory.

Morfet [40–42] proposed a new formula:

$$Q = \frac{K_M\left(\rho u_*^3 - \rho u_{+cr}^3\right)^{3/2}(\sin\theta_b)^{3/4}}{g\,(\rho_s - \rho)\,D_{90}^2} \tag{14}$$

where K_M is a calibration coefficient equal to 2.84×10^{-5}, $\rho u_*^3 - \rho u_{+cr}^3$ is the strength of the virtual wave, u_{+cr} is the velocity in critical or threshold wave conditions for sediment movement, θ_b is the angle between the wave front and the coastline in breaking, and u_* is the dissipation velocity, shown as

$$u_* = \left(\frac{D_d}{\rho}\right)^{1/3} \tag{15}$$

with D_d being the energy dissipation rate of waves, which can be used as a factor of LST instead of current power and can be found by using

$$D_d = \frac{\rho\, g^{3/2}\, H^{5/2}}{4\ L} \tag{16}$$

where L is the wavelength (m), and H is the representative wave height (m) at the breaking zone.

2.2. Methods of Balancing Forces

This method indicates that LST is connected to the lowest shear stresses. It requires a prior hydrodynamic formulation for radiation-induced currents caused by waves. Consequently, in comparison to the energy technique and the dimensional analysis method, it is more intricate (and difficult to solve). Out of all the calculations that were not evaluated using Shoreham's data, the balance of forces equation is the most precise.

Subsequently, Bijker [22,23] improved the use of hydrodynamic methods by numerically integrating the rate of transportation in the surfing area. It should be noted that they did not propose a new LST equation.

Damgaard and Soulsby [24] combined the hydrodynamic method with the balance of forces method to determine total LST. In order to do this, they introduced simplifications and assumptions, such as (a) homogeneous beach circumstances, (b) a roller in a shallow sea, (c) a regular rupture indicator, (d) no refraction in the surfing area, and (e) the gradient of radiation stress balanced by the shear force at the bottom. They obtained a resultant analytic expression for Q (total longshore transport rate), which is a combination of current-dominated transport, Q_1, and wave-dominated transport, Q_2. It also considers the current angle, θ_m, and the wave angle, θ_w:

$$Q = sign\{\theta_b\} \cdot max\{|Q_1|, |Q_2|\} \tag{17}$$

$$\theta_{max} = \sqrt{(\theta_m + \theta_w\cos\phi)^2 + (\theta_w\sin\phi)^2} \tag{18}$$

$$\phi = \frac{\pi}{2} - \theta_b \tag{19}$$

where the threshold condition is $Q = 0$ for $\theta_{max} \leq \theta_{cr}$, θ_{max} is the direction of the shear stress vector maximum, which is the result of a component mean, θ_m, and an oscillatory part, θ_w, resulting from the incoming wave, and θ_{cr} is the threshold angle for $Q = 0$.

The methodology of Damgaard and Soulsby [24] will not be included in the present study due to the high complexity of its formulation and the requirement of data that are not available for its treatment.

Wilson [43] used the following wave-induced friction factor (f_w) for moving bed and laminar flow conditions as a parameter for the calculation of wave-dominated transport Q_2:

$$f_{w,sf} = 0.0655\left(\frac{\varphi_b \cdot H}{g}\right)^{1/5}(\pi \cdot (s-1) \cdot T)^{-2/5} \tag{20}$$

where H represents the depth (m), s is the relative density, T is the representative wave period (s), and φ_b is the surf zone's constant ratio of wave height to depth.

2.3. Dimensional Analysis Methods

The set of dimensional formulas was created from multiple regression analysis, and some dimensionless parameters are considered important in LST. These equations are similar in shape to the energy methods but were calibrated and validated experimentally without considering the van Wellen energy approach [1].

Damgaard and Soulsby's [24] and Soulsby's [25] formulas, based on laboratory data from 1994 and input from van Hijum and Pilarsick [26], showed reliable results on coarse-grained beaches. In this case, Hs was used in the equations.

These equations were derived from dimensionless mathematical parameters rather than physical principles. From the data obtained from laboratory tests carried out by van Hijum and Pilarsick [26] and van Hijum [27], the following expression was obtained:

$$\frac{Q}{g\,D_{90}^2\,T_s} = 7.12 \times 10^{-4}\frac{H_{sd}(\cos\theta_b)^{1/2}}{D_{90}}\left[\frac{H_{sd}\,(\cos\theta_b)^{1/2}}{D_{90}} - 8.3\right]\frac{\sin\theta_b}{\tanh\left(\frac{2\pi d}{L}\right)} \tag{21}$$

where H_{sd} is the significant wave height, and d is the water depth, and T_s is the wave period (in s).

The term $B = \frac{H_{sd}\,(\cos\theta_b)^{1/2}}{D_{90}} - 8.3$ of Equation (21) must be greater than zero. Otherwise, Q would be zero or negative. Likewise, Brampton and Motika [10] pointed out that this term should be raised to a power greater than one to represent LST with high levels of wave energy.

Veinticlós-22

For sandy beaches, Kamphuis et al. [28] developed an LST equation that includes the slope of the beach ($\tan\alpha$) and D_{50}:

$$Q = 1.28\,\frac{\tan\alpha\, H_{sb}^{\frac{7}{2}}}{D_{50}}\sin 2\theta_b\,, \quad \left[\frac{kg}{s}\right] \tag{22}$$

Equation (22) can also be applied to coarse-grained beaches, according to extensive laboratory data, with H_{sb} being the significant wave height in the breaking condition.

Van der Meer [30] reanalyzed the information from van Hijum and Pilarsick [26] and proposed the following equation:

$$Q = 0.0012\, g\, D_{n50}\, T_p\, H_s\sqrt{\cos\theta_b}\left(\frac{H_s\sqrt{\cos\theta_b}}{D_{50}} - 11\right)\sin\theta_b \quad [kg/s] \tag{23}$$

where

$$D_{n50} = \left(\frac{M_{50}}{\rho_s}\right)^{1/3} \tag{24}$$

M_{50} is the average weight of the sediment, and T_p is the peak wave period.

Kamphuis [29] refined the equation from additional experiences in hydraulic models.

$$Q = 2.27\, H_{sb}^2\, T_p^{1.5}\, m_b^{0.75}\, D_{50}^{-0.25}\sin^{0.6} 2\theta_b \quad [kg/s] \tag{25}$$

Subsequently, Kamphuis [29] found Equation (26) to be valid for LST on sandy beaches when contrasted with the field data and laboratory experiments. However, for coarse-grained beaches, the results can exceed this by two to five times. This is because gravel beaches absorb a greater amount of wave energy as they filter through the grains.

The annual LST is estimated by using the following:

$$Q = 63433\,\chi_{Kamphuis}\,, \quad \left[m^3/year\right] \tag{26}$$

where

$$\chi_{Kamphuis} = \frac{1}{(1-p)\,\rho_s}\frac{\rho}{T_p}\,L_o^{1.25}\,H_{sb}^2\,m_b^{0.75}D_{50}^{-0.25}\sin^{0.6}2\theta_b \tag{27}$$

with p representing the porosity index and L_o representing the deepwater wavelength. m_b is the beach slope.

While considering the precision of the expected rates of transportation during hurricanes, the following alternate rendition is proposed:

$$Q = 50000\,\chi_{Kamphuis}\,, \quad \left[m^3/year\right] \tag{28}$$

Van der Meer and Veldman [44] indicated that Equation (23) can be simplified to

$$Q = 0.0012\,\pi\, H_s\, C_{op}\sin 2\theta_b, \quad (gravel\ and\ sand\ beaches) \tag{29}$$

where C_{op} is the peak deepwater celerity wave = $gT_p/2\pi$. For breakwater barriers and angles of 15–40°, we have $\frac{H_s}{\Delta D_{n50}} < 10$, with Δ being the relative specific weight of the submerged solid material.

$$Q = 0 \text{ for } H_o\,T_{op} < 105$$

$$Q = 0.00005\,(H_o\,T_{op} - 105)^2 \tag{30}$$

Here, H_o is the deepwater wave height (m), and T_{op} is the deepwater peak wave period (s).

Mil-Homens et al. [45] and Kamphuis [29] concluded that, to reduce the bias to zero and the $RMSE$ value to around 0.40 (close value to the noise in the statistics present from

validated information), this could be achieved by using multiple regression and varying the exponents of Kamphuis' formula, obtaining the following equation:

$$Q = 0.15\,\frac{\rho_s}{\rho_s - \rho}\,T_p^{0.89}\,m_b^{0.86}\,D_{50}^{-0.69}\,H_{s,br}^{2.75}\sin^{0.5}2\theta \tag{31}$$

where $H_{s,br}$ is the significant wave height in the breaking condition.

Then, by gathering field data, van Rijn [46] proposed a formula for LST known as the CROSMOR framework, which applies to sandy, as well as gravelly, beaches.

$$Q = 0.00018\,\rho_s\,g^{0.5}\,m_b^{0.4}\,D_{50}^{-0.6}\,H_b^{3.1}\sin 2\theta_b \tag{32}$$

where H_b is the wave height in the breaking condition and m_b is the beach slope.

The CROSMOR model gives slightly increased findings (by a factor of 1.5) about the storm circumstances' (high-energy circumstances) measurement values. Additionally, in low-wave circumstances, it produces lower results (by a factor of 2). When dealing with swell-type wave situations, the quasi-regular wave technique yields the greatest results. The lack of coastal transport in the oscillation zone could be the reason for the underprediction for low-wave situations.

2.4. Summary of the Different Formulations

In order to summarize the various methodologies cited in this work, the methods with the most important hypotheses and the field of validity of each of these are described in Table 1. Column 1 shows the LST calculation method type, column 2 the author(s) and reference, column 3 the hypotheses, and column 4 the formula validity field.

Table 1. Summary of the main formulas of LST.

1. Type	2. Method	3. Hypothesis	4. Field of Validity
Energy Flux	CERC [5]	The longshore wave power per beach length is directly related to the LST - immersed weight sediment transport rate, or I.	The CERC formula overpredicts transport rates for particle sizes and beach slopes, and significant tidal current velocities prevent its application.
	Swart [7]	Addition of a variable, K, as a function of D_{50}.	Despite its reliance on the grain diameter, [12] discovered that the equation by Swart was unable to provide a dependable K, even within the range 0.1 mm < D_{50} < 1 mm.
	Chadwick [9]; Brampton and Motyka [10]	A significantly lower value for K, Brampton and Motyka [47], limiting the significant breaking wave height to 0.5 m or less, and treating ε_1 and ε_2 as zero.	The normal CERC equation yielded a K value of 7% for sand, contrasting with a 9% K value obtained using Equation (8) with threshold and particle size terms.
	Schoonees and Theron [11,12]	The study found a low correlation coefficient for D_{50} > 1 mm in an energy-flux expression, suggesting that shingle transmission becomes more efficient when an energy threshold is surpassed.	Electronic shingles showed higher transport rate than aluminum tracers, suggesting a potential underestimate of transmission efficiency due to lack of transport data in high-energy situations.
Current Energy	Bailard [18]	It considers both bed load and suspended load, since coarse-grained beaches are unlikely to experience suspended sediment transfer.	It does not take into consideration the influence of the movement threshold. Therefore, applying it to beaches with coarse grains could lead to an overestimation of the overall longshore transport rate.

Veintiuno - 21

Table 1. *Cont.*

1. Type	2. Method	3. Hypothesis	4. Field of Validity
	van Hijum and Pilarczyk [26]	The Delft coastal transport equation, based on laboratory tests, suggests sediment movement starts when square brackets exceed one, but higher wave energy levels require a higher threshold term.	This Equation (21) presents challenges in predicting LST due to wave characteristics varying between offshore and beach locations, causing errors in inshore measurements.
	Kamphuis et al. [28]	The methodology, developed through field data and laboratory experiments, may be applicable to beaches with coarse-grained sediments, considering beach slope and grain size impact.	The LST formula of Kamphuis et al. It was created for use on sandy and coarse-grained beaches.
	van der Meer [30]	This equation reanalyzed the data from former studies [27] after realizing how difficult it was to obtain the necessary parameters for the original Delft equation.	Equation Chadwick (1989) [9] and this one are very similar. Primarily, this one is different in that the threshold term and the constant's value have been slightly altered.
Dimensional Analysis	Kamphuis [29]	Kamphuis refined his formula using hydraulic models, validating it for field and laboratory sand transport rates, and comparing it to coarse-grained beaches.	Grain size and beach slope are included in Equation (25). These two components tend to cancel each other out as grain size increases on beaches with reduced slopes.
	van der Meer and Veldman [44] for $H_s/(\Delta D_{50})$	A statement for the longshore transportation of gravel and rock beaches. The kind of structure (sand, shingle, rock, or berm breakwater) and the wave climate affect longshore transit.	According to [43], Equation (29) should only be used for rock/gravel beaches (berm breakwater) at angles between 15 and 40° and only within $10 < H_s/D_{50}$.
	Mil-Homens et al. [45]	The study modified the coefficients of Kamphuis' formula to reduce bias to zero and *RMSE* to 0.40, resulting in Equation (31).	The Mil-Homens formula overlooks the impact of submerged sand bars near the coast, which can significantly influence wave breaking and LST calculation, unlike a representative Dean profile.
	van Rijn [46]	The CROSMOR model, a formula for longshore transport (LST) based on 22 field-data gatherings, analyzes wave height, wave incidence angle, and longshore transport.	The data set was used to analyze wave period, profile shape, and particle size, resulting in a common formula for gravel and sand LST.

2.5. *CoastSat Software Method*

The free software CoastSat was used for the calibration and validation of this methodology. It is a Python program (using the Anaconda 3 environment manager). This allows users to obtain a time series of shorelines for any coast in the world, starting 39 years ago (and increasing) from the Sentinel 2 and Landsat missions. With these satellite images and the CoastSat software Vos et al. [48], the evolution of the coastline is determined computationally, Figure 4.

With this digital information on the temporal evolution of the coastlines, the area of advance or retreat of all of them is calculated given a baseline defined by the researcher. With this same baseline, closed polygonal areas are generated for all the coastlines of the different images used by CoastSat. Then, with the temporal evolution of the areas and with the help of the Birkemeier closure depth [49], the volumes of accretion or erosion are

calculated, and these volumes are divided by the elapsed time interval of each of them, finally obtaining the average LST in m^3/s. The equation used is the following:

$$Q = \sum Q_k \text{ and } Q_k = \frac{\Delta A_k}{\Delta t_k} D_s (33)$$

where $A = \sum A_k = \sum \Delta x_k \cdot \Delta y_k$, and thus, A is the variation in the total surface of the beach.

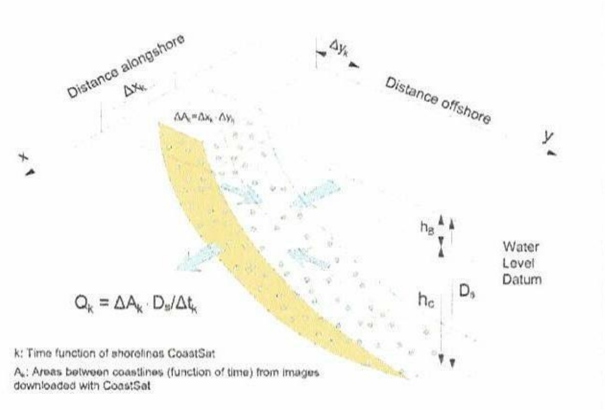

Figure 4. The conservation equation LST (Pernald-Considere) [50] used with the images downloaded from CoastSat.

Moreover, $D_s = h_B + h_C$ is the sum of the height of the emerged beach or berm (h_B) plus the Birkemeier closure depth (h_C) (see Figure 4).

Finally, the area A_k is the area between the current coastline k and a base coastline (selected by the researcher, but behind the entire group of coastlines of the beach). N = the quantity of coastlines discharged between the years 2016 to 2022. Thus, we have n-1 areas $\Delta A_k = A_{k+1} - A_k$ in each interval of time Δt_k.

Q_k is the LST in m^3/sec for each ΔA_k, obtaining Q_{n-1} LST flows in total. And to obtain the average annual flow, all the Q_k Δt_k are added together and this final volume of sediments is divided by the interval of time between the downloaded images (2016–2022). This process included the dredging volumes carried out during the years under study.

As for the boundary of the artificial structure (breakwater), the CoastSat method is true in that $Q_L = 0$, and Equation (33) only determines the advance or retreat (sedimentation or erosion) that accumulates in the entire southern area of the breakwater.

As a deficiency of this CoastSat method, we can mention that the calculation depends on the sub-pixel resolution of the images (10 m approx.) and that the LST can only be determined a posteriori, according to the availability of existing historical images of the study area. The hydrodynamic variables to estimate the LST calculations were obtained from the study [51].

3. Results and Discussion

A comparison of LST in the port of Salaverry was made according to the calculations of the different methodologies with the results of the processing of the CoastSat software. The main advantages and disadvantages of each method are pointed out. The results are shown in Table 2. Column 1 shows the type of method, and column 2 shows the author(s).

Veinte-20

Columns 3 and 4 show the advantages and disadvantages observed during the use of the various calculation methodologies for LST.

Table 2. The application of the main formulas of LST to the case of the Port of Salaverry in Peru. The main advantages and disadvantages of each method are pointed out.

1. Type	2. Method	3. Advantages	4. Disadvantages
CoastSat Value	CoastSat applied to satellite images	Real data	This method can only be used a posteriori, after having satellite images available.
Energy Flux	CERC [5]	• Flexibility: the CERC formula is adaptable to various conditions and can address problems also solvable by the Bijker formula; • Accuracy: it effectively predicts sedimentation in narrow channels without breaking waves, aiding in hydraulic engineering project planning; • Simplification: the CERC formula streamlines the calculation of longitudinal sediment transport, enhancing its practical applicability.	• Limitations: the CERC formula solely considers the sign of function values in its approximations, neglecting their magnitude; • Complexity: implementing the CERC formula can be challenging, particularly for individuals lacking experience in mathematical modeling; • The accuracy of the CERC formula is contingent upon the quality and quantity of data used for calibration, which may pose challenges in certain situations.
	Swart [7]	• Simplicity: it is easy to apply and only requires measurements of wave height and wave incidence angle; • General applicability: it has been used in a wide range of coastal conditions, including sand and gravel; • 3. Flexibility: it can be used to predict transport in different wave and sediment conditions.	The Swart formula has limitations, including limited precision, reliance on data quality, and not considering all processes affecting longshore sediment transport, such as current velocity and water depth.
	Chadwick [9]; Brampton and Motyka [10]	• Precision: the Chadwick formula has been verified through field measurements and numerical modeling, indicating good precision in estimating longshore transport; • General applicability: the formula has been applied to different wave and sediment conditions, making it useful for a wide range of situations; • Flexibility: The formula can be used to predict transport in different wave and sediment conditions.	• Limited precision: the Chadwick formula may inaccurately estimate transport in specific conditions, especially in high wave or coarse sediment scenarios; • Dependence on data quality: the accuracy of results is contingent upon the quality and quantity of calibration data; • Does not consider all processes: the formula does not include all processes that influence longshore sediment transport, such as longshore current velocity or water depth.
	Schoonees and Theron [11,12]	This formula, based on 270 global data sets, offers superior accuracy compared to the Shore Protection Manual, achieving a standard error of 0.515.	This formula, despite its potential, has limitations for coarse sediments due to the variability of the calibration coefficient.
Current Energy	Bailard [18]	The formula is simple, precise, and generally applied, requiring minimal complex data, and is verified through field measurements and numerical modeling for estimating longshore transport.	The formula's precision is limited due to potential underestimation in high wave or coarse sediment situations, insufficient consideration of longshore current velocity, or water depth.

Table 2. *Cont.*

1. Type	2. Method	3. Advantages	4. Disadvantages
Dimensional Analysis	van Hijum and Pilarczyk [26]	• Precision: the formula has been verified through field measurements and numerical modeling; • General applicability: the formula has been applied to different wave and sediment conditions, making it useful for a wide range of situations; • Flexibility: the formula can be used to predict transport under different wave and sediment conditions.	The formula has limited precision, may underestimate transport in high wave or coarse sediment situations, does not consider all processes, and may not be as precise as other formulas.
	Kamphuis et al. [28]	The formula offers superior precision in fitting field data compared to the Shore Protection Manual, incorporating critical parameters affecting longshore transport, primarily validating for sandy beach conditions.	The Kamphuis formula, while effective for gravel and pebble beaches, has limitations due to low complexity and reliance on low-quality field data, making it challenging to predict alongshore transport under high-energy wave conditions.
	van der Meer [30]	• Precision: the formula has shown a good fit to field data in moderate wave and fine sediment conditions; • Flexibility: the formula can be used to predict transport in different wave and sediment conditions; • Applicability: the formula has been validated in a wide range of coastal sites and climatic conditions.	The formula's precision is limited in high wave and coarse sediment conditions, and its accuracy is influenced by data quality, making it less precise than alternative models.
	Kamphuis [29]	• Accuracy: under moderate wave and fine sediment conditions, the formula has demonstrated an excellent fit to field data; • Flexibility: predicting movement under various wave and sediment conditions is possible using this approach; • Applicability: a variety of coastal locations and climates have been used to validate the algorithm.	The formula's precision is limited, underestimating longshore transport in high wave and coarse sediment conditions, and its accuracy depends on data quality, making it less reliable than alternative models.
	van der Meer and Veldman [44]	• Precision: in situations with moderate waves and fine silt, the formula has demonstrated a strong fit to field data; • Flexibility: using the method, one can forecast transport under various wave and sediment circumstances; • Applicability: the formula has been verified in a variety of coastal locations and climates.	The van der Meer and Veldman formula for predicting coastal performance has limitations, including inaccuracies, limited applicability, complexity, and neglect of long-term processes, requiring further research.
	Mil-Homens et al. [45]	The formula improves precision and applicability across wave and sediment conditions, including sandy and gravel beaches, and is validated using a comprehensive field data set.	The Mil-Homens et al. (2013) formula for longshore sediment transport has limitations, such as empirical nature, calibration sensitivity, and data requirements, requiring further refinement or alternative models.
	van Rijn [46]	The van Rijn formula for longshore sediment transport is user-friendly, versatile, and accessible, incorporating wave height and sediment characteristics, and useful for coastal management and engineering projects.	The van Rijn formula for longshore sediment transport has limitations due to its empirical basis, limited sediment size range, uniform conditions, and data-intensive nature.

The data in Table 3 depend on the temporal availability of the LandSat and Sentinel 2 missions in the Salaverry port area. The sum of all these areas gives us the LST area in

Diecinueve - 19

According to van Rijn [46], his Equation (32) provides good results between the calculated and measured values in moderate wave conditions and fine sediments. It also includes key parameters that influence the LST, such as grain size, beach slope, and wave height. Therefore, it is applicable to a variety of coastal sites and climatic conditions. For our particular case, it is observed that the error, compared to that calculated by the CoastSat method, is 20%. As a disadvantage, it can be pointed out that the formula is not always accurate in extreme conditions, such as very high waves or very coarse sediment size.

3.4. General Summary

As we can see in Figure 4, the results of the methods that come closest to the results obtained with CoastSat are van Rijn [46], Swart [7], and van der Meer [30], with 20%, 4%, and 0%, respectively. The methods of CERC [5], Schoonees and Theron [11,12], and van Hijum and Pilarczyk [26] are very far from the result obtained with CoastSat (−84%, −92%, and −96%, respectively), Figure 5.

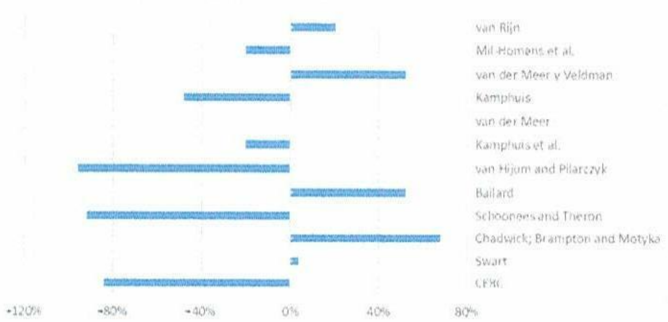

Figure 5. The error of the different formulas used related to the CoastSat results for Salaverry Beach (Peru).

Energy-flux methods for calculating LST are predicated on the principles of wave energy dynamics as they interact with coastal environments. The most prominent approach, the energy-flux method (CERC), leverages the parallel component of wave energy flux to establish a linear correlation between sediment transport and energy input, encapsulated in the equation ($Q = K \cdot P_{ls}$), where (Q) represents LST and (P_{ls}) is energy flux.

The current energy methods for estimating LST are grounded in the interaction between hydrodynamic forces and sediment dynamics along coastal environments. These methodologies primarily focus on the energy imparted by currents, particularly those generated by wave action and tidal influences, to predict sediment movement.

Regarding dimensional analysis methods, it can be stated that these are derived from dimensionless parameters and use physical variables calibrated through laboratory and field experiments.

The formulation of van Hijum and Pilarczyk [26] and van Hijum [27], following Brampton and Motyka [10], indicated that their term defined in Equation (21) as A should be used for the high energy levels of the waves producing the LST. The results obtained with this equation generate an error of −96% compared to that obtained with CoastSat. At the same time, this formulation introduces numerous variables, complicating its calculation.

Van der Meer [30] reanalyzed the data of van Hijum and Pilarczyk [26], generating a new formula introducing D_{50} instead of D_{90}. This is a simple formula to calculate and has an error of 0% with respect to that obtained with CoastSat. Furthermore, van der Meer and Veldman [44] proposed Equation (29), which can be used for gravel and sand beaches, although the results generate a higher error, on the order of 46%.

Van Rijn [46] collected field data from 22 experiences, and proposed his Formula (32) for LST, giving rise to the CROSMOR model, which is applicable to sand and gravel beaches. This is a simple formula and results in a variation of only 20% in the calculation compared to that obtained by CoastSat.

It should be noted that, in this work, several calibration procedures of the cited LST methods are summarized, for example, the creation of sedimentation pools, littoral drift roses, gravel traps, tracers, samplers, tip growth, or breakwater accretion, among others (Walton and Dean [53]). Regarding the cost of implementing these calibration methods, it is noted that this can vary considerably. This depends on several factors, such as the scale and complexity of the study, the geographic location, and the equipment and technology used, as well as the costs associated with specialized personnel, logistics, and duration of the study. In the present validation carried out with CoastSat, the costs are much lower, since it would not be necessary to have workers or civil works, personnel, and equipment displacement. In our proposal, only a good computer and the CoastSat software are needed, which is freely available and considering that satellite images are also free. Furthermore, compared to traditional calibration methods, this low-cost methodology does not experience a significant loss of accuracy.

It is worth mentioning that there are still places where not many coastal satellite images are available. Not all available images have the same temporal and spatial resolution, which limits the ability to obtain more accurate results in these coastal areas. Both considerations make the calculation of LST difficult. In addition, global sea-level rise is a critical issue in coastal areas, requiring accurate estimation of coastal retreat and sand volume to address the sediment deficit. However, a specific methodology has not yet been developed [54].

Even so, the use of satellite data through comparison software (e.g., CoastSat) is recommended as a validation method for LST studies.

Finally, from the analysis carried out, it can be observed that all the formulations of the three LST categories present results with a wide variation, even greater than 90%. This is possibly due to the fact that the equations use very diverse parameters and variables.

With the results obtained from Table 4, an average LST value of 0.029 m^3/s was determined, with a relative standard deviation of 46.63% and a standard deviation of 0.0135. However, this average value was obtained for a wide range of LSTs and may not be significant. The value calculated through the CoastSat method was 0.0254 m^3/s for Salaverry Beach in Peru.

4. Conclusions

CoastSat uses real satellite images with good resolution at a sub-pixel level, which provides a real image of the variation of the coastline applied to many coastal environments. In addition, it is widely used to determine shorelines by many researchers, due to its very low computational complexity and high data availability for its calculation in most cases. The uncertainty in the parameters is minimal given the scaling factor of the images and their good resolution. In this work, the LST calculation was carried out using the CoastSat method, which only requires freely accessible satellite images. The result was an LST of 0.025 m^3/s.

The energy flow methods were analyzed, observing that the Swart equation has a good agreement, with an error of 4% with respect to the calculation with the CoastSat method. While the CERC requires less data and is very simple, errors increase when not including important variables in the determination of the LST, such as the slope of the beach and the wave period. For the present case, the error was −84%.

While formulas such as CERC, Swart, Chadwick, Schoonees, and Theron offer a low computational complexity and acceptable data availability, their predictive accuracy benefits from high-quality in situ measurements. However, inaccurate LST predictions for

Dieciocho – 18

Diecisiete- 17

the design and maintenance of coastal structures imply higher economic investments and a pressing need for cost-effective calibration methodologies.

Using the current energy method proposed by Bailard [18], an error of 52% was obtained with respect to that calculated by CoastSat. This equation is very simple, requiring data that are easy to obtain. But, it does not consider variables such as depth or current speed.

As for the force balance methods, they have the disadvantage of using complex formulations, and they require parameters that are difficult to quantify in reality.

Dimensional analysis methods for predicting longshore sediment transport (LST) are significantly influenced by the quality and representativeness of the field data, particularly under high-energy wave conditions, where data acquisition is challenging. Among these, van Rijn's method demonstrates a 20% error relative to the CoastSat calculations and incorporates essential factors, such as beach incline, sediment density, median diameter, and breaker wave height, making it suitable for sandy and gravel beaches. In contrast, the van der Meer formula yields a 0% error but is not recommended for gravel and pebble beaches. Other methodologies exhibit substantial errors, ranging from 20% to over 90%, compared to CoastSat results.

The main disadvantage of the CoastSat method is that it can only be used a posteriori after having satellite images available. This study proposes to improve the existing approaches by integrating digitized satellite imagery using remote-sensing techniques to improve LST calibration while addressing the economic constraints faced by many countries.

Author Contributions: Conceptualization: J.J.M.-P., B.J.-A., C.M.A.-C., C.A.Q.-G.; Methodology: B.J.-A., J.J.M.-P., C.M.A.-C., C.A.Q.-G., D.D.S.-J., A.C.-d.-V.; Software: C.M.A.-C., A.C.-d.-V.; Validation: B.J.-A., J.J.M.-P.; Formal Analysis: C.M.A.-C., A.C.-d.-V., C.A.Q.-G., D.D.S.-J.; Investigation: B.J.-A., J.J.M.-P., C.M.A.-C.; Resources, B.J.-A., J.J.M.-P.; Data Curation: C.M.A.-C., A.C.-d.-V.; Writing—Original Draft Preparation: C.M.A.-C., C.A.Q.-G., D.D.S.-J.; Writing—Review and Editing: B.J.-A., J.J.M.-P., A.C.-d.-V.; Visualization: C.M.A.-C., A.C.-d.-V.; Supervision: B.J.-A., J.J.M.-P., C.A.Q.-G.; Project Administration: B.J.-A., J.J.M.-P.; Funding Acquisition: J.J.M.-P., B.J.-A.. This research is part of the Doctoral Thesis of PhD Student Cesar Alpaca Chacón. All the authors contributed to the writing and supervision of the manuscript, as well as discussing the results. Each writer has examined and accepted the published version. All authors have read and agreed to the published version of the manuscript.

Funding: This research was partially funded by: Junta de Andalusia and European Union (Recovery, Transformation and Resilience Plan), grant number PCM_00124, and RNM912 Research Group belonging to the University of Cádiz.

Acknowledgments: To H&O Ingenieros Consultores S.A. and DHN for their greater willingness to support this study by providing relevant information.

Conflicts of Interest: The authors declare no conflict of interest.

Notation

c	Wave celerity (m/s)
C_g	Group celerity (m/s)
C_{op}	Peak deepwater celerity wave (m/s)
d	Depth of water (m)
$D_{(50/90)}$	(50/90%) Grain diameter representative (m)
D_d	Rate of wave energy dissipation (W/m^2)
e	Ratio of voids
E	Density of waves (kg/s^2)
$f_{w,sf}$	Friction factor for wave-induced rough turbulent flow
g	Acceleration due to gravity (m/s^2)
h	Depth (m)
$f_{w,t}$	Friction factor for rough turbulent flow induced by waves

H	Wave height representative (m)
H_{rms}	Root-mean-square wave height (m)
H_s	Significant wave height (m)
I	Total mass rate of coastal transport (Kg/s)
I_{ls}	Coastal transport rate for total submerged weight (N/s)
k	Wave number (m^{-1})
$K_{1,2,3}$	Coefficients of proportionality
L	Wavelength (m)
L_o	Deepwater wavelength (m)
M_{50}	50% of a unit's medium mass is indicated on the mass distribution curve (kg)
m_b	Beach slope (m/m)
n	Quantity of observations
p	Porosity index
P_*	Power from virtual waves (kg/s^3)
P_{ls}	Coastal wave power flow (W/m)
P_{ls0}	Coastal wave energy threshold value flow (W/m)
Q	Total volumetric rate of coastal transport (m^3/s)
Q_1	Integrated long-distance coastal transport rate under current conditions (m^3/year)
Q_2	Integrated coastal transport rate along the coast in circumstances where waves predominate (m^3/year)
q	Rate of volumetric load transport (m^3/(m s))
R	Coefficient of correlation
s	Comparative density
T	Typical wave duration (s)
T_{op}	Deep water peak wave period (s)
T_p	Peak wave period (s)
T_s	Significant time of wave (s)
T_z	Zero cross wave period (s)
u_*	Rate of dissipation (m/s)
u_{*cr}	Velocity in critical (threshold condition of wave for sediment movement, m/s)
U_{mb}	Maximum speed in orbit at the bottom (m/s)
w_s	Sediment fall speed (m/s)
b	Subscript indicating values sampled at the wave's breaking point
C_r	Subscript signifying important values
d	Sampled data at the point when the water depth equals d are indicated by a subscript
m	Subscript representing mean values
max	Subscript indicating the highest values
sb	Subscript indicating significant wave height in breaking
sd	Subscript indicating significant wave height in the water depth d
w	A subscript representing values caused by waves
α	Beach gradient (rad)
Δ	Relative specific weight of the submerged solid material
$\varepsilon_b, \varepsilon_s$	Efficiency terms for suspended and bottom loading
$\varepsilon_2, \varepsilon_1$	Coefficients of calibration
γ_b	Wave's angle break index between the direction of the waves and the contours of the beach (°)
φ_b	Constant ratio of the surf zone of wave height to depth.
ϕ	Complementary angle of wave breaking angle (°)
Γ	Factor of conversion between volumetric and mass transport rates (kg/m^2 s^2)
θ_b	Angle between the wave front and the coastline (°)
ρ	Fluid density (kg/m^3)
ρ_s	Sediment density (kg/m^3)
σ	Error in relative standard of estimation

References

1. Van Wellen, E.; Chadwick, A.J.; Mason, T. A review and assessment of longshore sediment transport equations for coarse-grained beaches. *Coast. Eng.* **2000**, *40*, 243–275. [CrossRef]

2. Bennis, A.-C.; Furgerot, L.; Du Bois, P.B.; Dumas, F.; Odaka, T.; Lathuilière, C.; Filipot, J.-F. Numerical modeling of three-dimensional wave-current interactions in a complex environment: Application to Alderney Race. *Appl. Ocean Res.* **2020**, *95*, 102021. [CrossRef]
3. Calvino, C.; Dabrowski, T.; Dias, F. A study of the wave effects on the current circulation in Galway Bay, using the numerical model COAWST. *Coast. Eng.* **2023**, *180*, 104251. [CrossRef]
4. Ardhuin, F.; Roland, A.; Dumas, F.; Bennis, A.C.; Sentchev, A.; Forget, P.; Wolf, J.; Girard, F.; Osuna, P.; Benoit, M. Numerical wave modeling in conditions with strong currents: Dissipation refraction relative wind. *J. Phys. Oceanogr.* **2012**, *42*, 2101–2120. [CrossRef]
5. Coastal Engineering Research Center (US). *USACE Shore Protection Manual Center UACER Editor*; USACE, Coastal Engineering Research Center (US): San Francisco, CA, USA, 1984.
6. Tomasicchio, G.; D'Alessandro, F.; Barbaro, G.; Malara, G. General longshore transport model. *Coast. Eng.* **2013**, *71*, 28–36. [CrossRef]
7. Swart, D.H. Predictive equations regarding coastal transports. In Proceedings of the 15th International Conference on Coastal Engineering, Honolulu, HI, USA, 11–17 July 1976; Engineers ASoC, Ed.; pp. 1113–1132.
8. Nicholls, R.J.; Wright, P. Longshore transport of pebbles: Experimental estimates of K. In *Coastal Sediments*; American Society of Civil Engineers: Reston, VA, USA, 1991; pp. 920–933.
9. Chadwick, A.J. Field measurements and numerical model verification of coastal shingle transport. In *Advances in Water Modelling and Measurement*; BHRA: The Fluid Engineering Centre: Cranfield, UK, 1989; pp. 381–402.
10. Brampton, A.; Motyka, J.M. Modelling the plan shape of shingle beaches. In *Estuarine Studies*; Conference, Sunderland Polytechnic: Sunderland, UK, 1984; Volume 12, p. 7.
11. Schoonees, J.S.; Theron, A.K. Review of the field database for longshore sediment transport. *Coast. Eng.* **1993**, *19*, 1–25. [CrossRef]
12. Schoonees, J.S.; Theron, A.K. Accuracy and applicability of the SPM longshore transport formula. In Proceedings of the 24th International Conference on Coastal Engineering, Kobe, Japan, 23–28 October 1994; pp. 2595–2609.
13. Inman, D.L.; Bagnold, R.A. *The Sea*; Hill, M.N., Ed.; Wiley-Interscience: New York, NY, USA, 1963; Volume 3, pp. 529–551.
14. Komar, P.D. The Longshore Transport of Sand on Beaches. PhD Thesis, University of California, Los Angeles, CA, USA, 1969.
15. Greer, M.N.; Madsen, O.S. Longshore sediment transport data: A review. In Proceedings of the 16th International Conference on Coastal Engineering, Hamburg, Germany, 27 August–3 September 1978; pp. 1563–1576.
16. Watts, G.M. *A Study of Sand Movement at South Lake Worth Inlet*; US Army, Beach Erosion Board: Washington, DC, USA, 1953; p. 42.
17. Caldwell, J.M. *Wave Action and Sand Movement Near Anaheim Bay*; Beach Erosion, Board: Washington, DC, USA, 1956; p. 68.
18. Bailard, J.A. A simplified model for longshore sediment transport. In Proceedings of the 19th International Conference on Coastal Engineering, Houston, TX, USA, 3–7 September 1984; American Society of Civil Engineers: Reston, VA, USA, 1984; pp. 1454–1470.
19. Bagnold, R.A. Beach and Nearshore Processes, Part 1: Mechanics of Marine Sedimentation. In *The Sea, Ideas and Observations*; N.Y.r Hill, Min.: New York, NY, USA, 1963; pp. 507–528.
20. Bagnold, R.A. *An Approach to the Sediment Transport Problem from General Physics*; US Geological Survey: Reston, VA, USA, 1966; Volume 422, pp. 11–137.
21. Frijlink, H.C. Discussion of the sediment transport formulas of Kalinske. In *Einstein, Meyer-Peter, and Müller about Recent Sediment Transport Measurements in Dutch rivers. 2me Journal Hydraulic*; Soc. Hydraulic de France: Paris, France, 1952; p. 98.
22. Bijker, E.W. *Some Considerations about Scales for Coastal Models with Movable Beds*; Delft Hydraulics Laboratory: Delft, The Netherlands, 1967.
23. Bijker, E.W. Mechanics of sediment transport by the combination of waves and current. In Proceedings of the Short Course Attached to 23rd International Conference on Coastal Engineering, Venice, Italy, 4–9 October 1992; pp. 147–171.
24. Damgaard, J.S.; Soulsby, R.L. Longshore bed-load transport. In Proceedings of the 25th International Conference on Coastal Engineering, Orlando, FL, USA, 2–6 September 1996; pp. 3614–3627.
25. Soulsby, R. *Manual of Marine Sands*; HR Wallingford: Oxfordshire, UK, 1994.
26. Van Hijum, E.; Pilarczyk, K.W. *Gravel Beaches: Equilibrium Profile and Longshore Transport of Coarse Material Under Regular and Irregular Wave Attack*; Delft Hydraulics Laboratory: Delft, The Netherlands, 1982; Publication no. 274.
27. Van Hijum, E. *Equilibrium Profiles and Longshore Transport of Coarse Material Under Wave Attack*; Delft Hydraulics Laboratory: Delft, The Netherlands, 1976; Publication no. 174.
28. Kamphuis, J.W.; Davies, M.H.; Nairn, R.B.; Sayao, O.J. Cálculo de la tasa de transporte de arena litoral. *Ing. Costera* **1986**, *10*, 1–21.
29. Kamphuis, J.W. Alongshore sediment transport rate. *J. Waterw. Port, Coastal, Ocean Eng.* **1991**, *117*, 624–640. [CrossRef]
30. Van der Meer, J.W. *Rock Slopes and Gravel Beaches are Under Wave Attack*; Technische Universiteit Delft: Delft, The Netherlands, 1990.
31. Schoonees, J.S.; Theron, A.K. Improvement of the most accurate longshore transport formula. *Coast. Eng.* **1996**, *1996*, 3652–3665.
32. Muñoz-Perez, J.J.; Gutierrez-Mas, J.M.; Parrado, J.M.; Moreno, L. Sediment transport velocity by tracer experiment at Regla Beach (Spain). *J. Waterw. Port Coast. Ocean Eng.* **1999**, *125*, 332–335. [CrossRef]
33. Holland, A. Mixed Sand and Gravel Beaches: Accurate Measurement of Active Layer Depth to Develop Predictive Models of Sediment Transport. Ph.D. Thesis, University of Sussex, Brighton, UK, 2019.
34. Verón, M.J.; Bértola, G.R. Aplicación del método de flujo de energía en el litoral de la provincia de Buenos Aires, Argentina. *Rev. Latinoam. Sedimentol. Análisis Cuencas* **2014**, *21*, 17–23.

35. Komar, P.; Inman, D. Longshore sand transport on beaches. *J. Geophys. Res.* **1970**, *75*, 5914–5927. [CrossRef]
36. Rosati, J.; Walton, T.L.; Bodge, K. Longshore sediment transport—Coastal engineering manual, Coastal and Hidraulics Laboratory (CHL), Engineer Research and Development Center (ERDC), Vicksburg, Mississippi. In *Part III, Coastal Sediment Processes*; Chapters 2–3; 2002; Available online: https://pdhonline.com/courses/c773/Part-III-Chap_2entire.pdf (accessed on 4 August 2024).
37. Smith, E.R.; Wang, P.; Zhang, J. Evaluation of the CERC formula using large-scale model data. In Proceedings of the Coastal Sediments, Coastal and Hydraulics Laboratory (CHL)—Engineer Research and Development Center (ERDC), Waterways Experiment Station, Vicksburg, MS, USA, January 2003; Volume 3.
38. Bray, M.J.; Workman, M.; Smith, J.; Pope, D. Field measurements of shingle transport using electronic tracers. In Proceedings of the MAFF Conference of River and Coastal Engineers, Loughborough, UK, 5–8 July 1996; pp. 10.4.1–10.5.3.
39. Tomasicchio, G.R.; Francone, A.; Salvadori, G. On the General Longshore Transport model for resilient beaches. *Coast. Eng.* **2023**, *180*, 104257. [CrossRef]
40. Morfett, J.C. Modeling shingle beach evolution. In *IAHR Symposium: Mathematical Modelling of Sediment Transport in the Coastal Zone*; Committee on Coastal and Maritime Hydraulics: Copenhagen, Denmark, 1988; pp. 148–155.
41. Morfett, J.C. The development and calibration of an alongshore shingle transport formula. *J. Hydraul. Res.* **1989**, *27*, 717–730. [CrossRef]
42. Morfett, J.C. *Shingle Movement on Groyned Beaches. Hydraulic and Environmental Modeling of Coastal, Estuarine, and River Waters*; U.S. Department of Energy, Office of Scientific and Technical Information: Reston, VA, USA, 1989; pp. 265–274.
43. Wilson, K.C. Friction of wave-induced sheet flow. *Coast. Eng.* **1989**, *12*, 371–379. [CrossRef]
44. Van der Meer, J.W.; Veldman, J.J. Singular points at berm breakwaters: Scale effects, rear, round head and longshore transport. *Coast. Eng.* **1992**, *17*, 153–171. [CrossRef]
45. Mil-Homens, J.; Ranasinghe, R.; de Vries, J.V.T.; Stive, M.J.F. Reevaluation and improvement of three commonly used bulk longshore sediment transport formulas. *Coast. Eng.* **2013**, *75*, 29–39. [CrossRef]
46. Van Rijn, L.A. Simple general expression for the longshore transport of sand, gravel, and shingle. *Coast. Eng.* **2014**, *90*, 23–39. [CrossRef]
47. Brampton, A.H.; Motyka, J.M. Recent examples of mathematical models of UK beaches. In *Coastal Sediments*; ASCE: Reston, VA, USA, 1987; pp. 515–530.
48. Vos, K.; Splinter, K.D.; Harley, M.D.; Simmons, J.A.; Turner, I.L. CoastSat: A Google Earth Engine-enabled Python toolkit to extract shorelines from publicly available satellite imagery. *Environ. Model. Softw.* **2019**, *122*, 104528. [CrossRef]
49. Birkemeier, W.A. Field data on seaward limit of profile change. *J. Waterw. Port Coastal, Ocean Eng.* **1985**, *111*, 598–602. [CrossRef]
50. Sánchez, J.C.; Mora, J.M.; Silva, R. *Dependencia Temporal de los Parámetros K1 y K2 Para La Predicción de la Evolución de Playas*; Instituto de Ingeniería, UNAM: Ciudad de Mexico, Mexico, 1998.
51. MTC-Consorcio Internacional AC-INC. Consultoría para la Elaboración del Estudio de Pre Inversión a Nivel Perfil para "Regeneración del Borde Costero de los Balnearios de las Delicias, Buenos Aires y Huanchaco". Informe Parcial 1, January 2014, 33-83. Available online: https://portal.mtc.gob.pe/transportes/acuatico/estudios.html (accessed on 4 August 2024).
52. Nicholls, R.J.; Birkemeier, W.A.; Hallermeier, R.J. Application of the depth of closure concept. *Coast. Eng.* **1996**, *1996*, 3874–3887.
53. Walton, T.L., Jr.; Dean, R.G. Longshore sediment transport via littoral drift rose. *Ocean. Eng.* **2010**, *37*, 228–235. [CrossRef]
54. Aguilera-Vidal, M.; Muñoz-Perez, J.J.; Contreras, A.; Contreras, F.; Lopez-Garcia, P.; Jigena, B. Increase in the Erosion Rate Due to the Impact of Climate Change on Sea Level Rise: Victoria Beach, a Case Study. *J. Mar. Sci. Eng.* **2022**, *10*, 1912. [CrossRef]

Dieciseis - 16

ARTÍCULO ORIGINAL

Revista de Investigación de Física **27(1)**, (Ene-Abr 2024)

Doi: 10.15381/rif.v27i1.27261

eISSN:1728-2977

Simulación numérica para representación de corrientes inducidas por oleaje. Aplicación al puerto de Ilo-Perú

César Alpaca *[1,2], Emanuel Guzmán[1], César Quispe[1], Juan Muñoz[2] y Bismarck Jigena[2]

[1] *Universidad Nacional Mayor de San Marcos, Lima, Perú*
[2] *Universidad de Cádiz, CASEM, España*

Recibido 30 Ene 2024 – Aceptado 31 Mar 2024 – Publicado 26 Abr 2024

Resumen

Este artículo tiene como objetivo representar las corrientes inducidas por oleaje en las zonas cercanas al puerto de Ilo, con el uso del software SMC (Sistema de Modelamiento Costero) y un programa de desarrollo propio en Matlab. En el presente estudio se utilizó para el módulo de oleaje la aproximación parabólica de RefDif, para un modelo de oleaje monocromático. El modelo numérico desarrollado en Matlab permite representar la hidrodinámica de olas y corrientes inducidas basado en las ecuaciones de Navier Stokes y conservación de masa, en forma diferencial con dos dimensiones espaciales (x, y) y una temporal (t). Este modelo se desarrolló tomando en consideración las variables promediadas en el eje vertical z y calado variable, considerando el fenómeno de shoaling y refracción que sufren las olas al acercarse a la zona costera de aguas poco profundas. El modelo desarrollado en Matlab se validó para caso simplificado de playas rectas. Al colocar un oleaje en direcciones Sur 30° Este, Este y Norte 30° Este, se observó que las corrientes inducidas por oleaje mantenían esas respectivas direcciones. Una vez validado el modelo desarrollado para caso simplificado, se corrió el programa para la batimetría de la zona cercana al puerto de Ilo. Validándose los resultados con data de campo obtenida con ADCP (Acoustic Doppler Current Profiler) con los del modelo y los resultados del software SMC inclusive. Se encontró una velocidad promedio del ADCP de 45.6 mm/s y una velocidad promedio del modelo SMC de 65.2 mm/s, mostrando una similitud del 70 % entre ambos valores. Los resultados de la simulación numérica muestran una desviación estándar en velocidades del 2 % para el punto de referencia del ADCP. Mientras que la desviación estándar de los datos del ADCP son de 24 %, para las velocidades resultantes.

Palabras clave: Simulación numérica de corrientes, olas, shoaling, refracción de olas.

*cesar.alpaca@unmsm.edu.pe

Numerical simulation for representation of wave-induced currents. Application to the port of Ilo-Peru

Abstract

The objective of this article is to represent the wave-induced currents in the areas near the port of Ilo, with the use of SMC software and a self-developed program in Matlab. In the present study, the parabolic RefDif approximation, for a monochromatic wave model was used for the wave module. The numerical model developed in Matlab allows representing the hydrodynamics of waves and induced currents based on the Navier Stokes equations and mass conservation, in differential form with two spatial dimensions (x, y) and one temporal (t). This model was developed taking into consideration the variables averaged in the vertical z axis and variable draft, considering the phenomenon of protrusion and refraction that the waves suffer when approaching the coastal zone of shallow waters. The model developed in Matlab was validated for the simplified case of straight beaches. By placing a wave in directions South 30° East, East and North 30° East, it was observed that the wave-induced currents maintained those respective directions. Once the model developed for the simplified case was validated, the program for the bathymetry of the area near the port of Ilo was run. Validating the results with field data obtained with ADCP (Acoustic Doppler Current Profiler) with those of the model and the results of the SMC software included. Finding an average speed of the ADCP of 45.6 mm/s and an average speed of the SMC model of 65.2 mm/s, showing a similarity of 70 % between both values. The modeling results show a standard deviation in velocities of 2 % for the ADCP reference point. While the standard deviation of the ADCP data is 24 %, for the resulting velocities.

Keywords: Modeling of currents, waves, shoaling, wave refraction.

Introducción

El puerto de Ilo está ubicado al sur del Perú en la costa del Océano Pacífico e inició actividades en 1970. Su plataforma tiene una altura de nivel medio de 5 m en pleamar; permitiéndole atender naves de hasta 35,000 DWT (Deadweight tonnage) en labores de embarque y desembarque de carga a granel, contenedores y minerales, hasta 1'400,000 TM por año [3] **APN** (2018). Hoy en día, las facilidades logísticas del puerto de Ilo no son suficientes comparados con otros puertos cercanos como Arica, Iquique o Antofagasta [4] Solís et al (2011).

Para que el puerto de Ilo pueda presentarse como una alternativa viable y real como puerto de entrada/salida para la carga comercial boliviana en el océano Pacífico, debe mejorar sus condiciones. En este aspecto, lo más importante es mejorar sus condiciones de navegabilidad de la dársena y de acceso al puerto, ya que actualmente tiene poca profundidad y está limitado a un calado de 11.00 m, lo que dificulta las condiciones de operatividad para buques de mayor calado y, por lo tanto, de mayor capacidad.

Por otro lado, también se debe mejorar la operatividad de los servicios de carga, descarga y estiba de la carga y la eficiencia de los servicios administrativos y de gestión del puerto. En cuanto al acceso al puerto deben mejorar sus vías de acceso, tanto por carretera como el acceso ferroviario. En su trabajo sobre el puerto de la Bahía de Cádiz, sur de España [5] (Jigena Antelo et al., 2023a) realiza un estudio de las condiciones de navegabilidad del puerto de Cádiz y de la operativa en su nueva terminal de contenedores, que dadas sus dimensiones se podría extrapolar al puerto de Ilo en Perú.

En este contexto, el estudio de corrientes en el puerto es importante porque ayuda a entender el impacto de la dinámica del oleaje en sus cercanías. Para ello, se realiza el estudio de corrientes en dos dimensiones espaciales (x, y) y una temporal (t), realizado con el modelo numérico SMC Mopla (Sistema de Modelamiento Costero, Morfología de playas, 2000) [6].

Tal como muestran diversas investigaciones, los estudios de corriente son importantes para los desarrollos portuarios. [7] Mahmoodi et al. (2020) en el puerto de Noshahr en Irán, costa sur del mar Caspio, identificó las principales razones de la sedimentación severa en la entrada de dicho puerto. Para ello, evaluó mediciones topobatimétricas e hidrodinámicas del área de estudio con el software DHI MIKE para determinar las corrientes inducidas por viento.

[8] Leys & Mulligan (2015) indican que en el puerto de Saint John de la bahía de Fundy ubicado en el Atlántico Canadiense, se generan enormes mareas a la salida de un río muy grande, produciéndose una sedimentación significativa de limo y arcilla, complicando la navegación y el dragado. Otro lugar, en la costa arenosa de la isla de Príncipe Eduardo en Darnley Inlet, se tiene un área expuesta a mareas y tormentas, sedimentando el área y afectando el canal de navegación. Con la recopilación de información de batimetría, nivel de agua, viento, olas y sedimentos, observación de accidentes geográficos erosivos/depositacionales, y fotografías satelitales, efectuaron

Quince-15

una simulación numérica hidrodinámica utilizando el modelo MIKE21, lo que también permite conocer los campos de corriente.

Todos estos estudios destacan una fuerte interacción de olas y corrientes. Tanto la zona de oleaje como los procesos de marea son clave para explicar correctamente la hidrodinámica [12] (Jigena-Antelo et al., 2015). Se observa que las corrientes y mareas afectan la ruptura de olas y la turbulencia del mar [13] Ardhuin et al. (2012).

[14] Olabarrieta et al. (2011) y [13] Ardhuin et al. (2012) muestran que la generación local de olas se ve afectada por las corrientes. A altas frecuencias, el desplazamiento Doppler inducido por la corriente puede ser significativo, y la advección de las ondas puede detenerse cuando se enfrentan fuertes corrientes adversas. Las corrientes también actúan directamente sobre el propio esfuerzo del viento generando el crecimiento de la ola. Sin embargo, no queda claro el rol de las corrientes en este proceso. [15] Renault et al. (2016) utilizan un modelo acoplado aire-mar para resaltar un complejo efecto retroactivo de las corrientes oceánicas sobre el viento en la capa límite de aire superficial.

[16] Guzmán (2006) realizó una simulación numérica del patrón de corrientes superficiales forzados por viento y marea en la bahía Ferrol-Chimbote, con el objetivo de determinar la influencia de dichas forzantes, dando así un diagnóstico del patrón de corrientes que serviría como contribución a la evaluación de recambio de aguas y su influencia en el proceso de contaminación en la bahía. Empleó el modelo POM (Princeton Ocean Model) para simular la corriente de marea, empleó como forzante los principales constituyentes armónicos de marea obtenidos del modelo global TOPEX6.0, los cuales fueron comparados con las predicciones de marea publicadas en Internet por la DHN (Dirección de Hidrografía y Navegación). Los resultados obtenidos muestran la influencia del viento y la marea en la generación de corrientes, concluyendo que, debido a la configuración morfológica de la bahía, la circulación que se presenta es muy lenta y que la marea ejerce mayor influencia en la circulación dentro de la bahía Ferrol, mientras que la influencia del viento es notoria fuera de la bahía.

[17] Varona & Aleman (1999) estudiaron la caracterización de las corrientes marinas por zonas en el tramo costero de Cazonal-Cazonalito (Cuba). Los datos fueron tomados de cuatro etapas oceanográficas. Se realizó la simulación del comportamiento de las corrientes de marea y, por último, fueron calculadas las corrientes inducidas por el viento. Concluyeron que predominan las corrientes residuales, con rumbos E y NE, y que son importantes las corrientes de marea, algo inestables en dirección. Sin embargo, deben analizarse cuidadosamente los resultados de los modelos numéricos e incluso contrastarse con experimentos in situ [18] Muñoz-Pérez et al. (1999), pues su uso por personal no experto puede conducir a errores drásticos [19] Gomez-Pina et al. (2007). Pequeñas variaciones en los parámetros de entrada pueden inducir resultados contradictorios en ciertas configuraciones batimétricas [20] Muñoz-Perez et al. (2010).

Metodología

Este artículo de investigación trata sobre las corrientes inducidas por oleaje en el puerto de Ilo. El modelo emplea las ecuaciones fundamentales de movimiento y continuidad en forma diferencial. Para la solución de estas ecuaciones se desarrolló un modelo en Matlab de diferencias finitas que permite determinar el campo de corrientes inducidas por el oleaje de la zona.

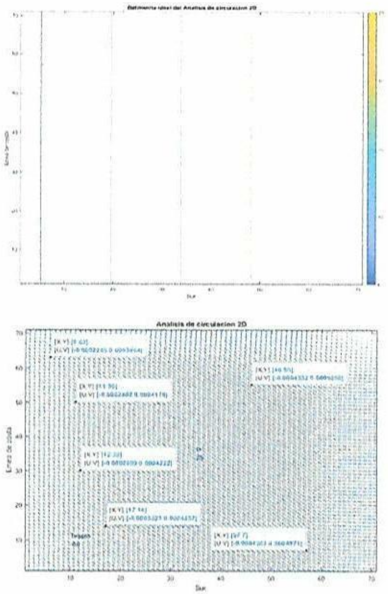

Figura 1: a) Batimetría recta de validación simplificada. b) Corrientes con ángulo de aproximación de -60° respecto al eje x de validación simplificada.

Los resultados de este modelo son validados primero para un caso simplificado de playas rectas. Encontrándose que las corrientes mantienen la dirección de aproximación del oleaje (Figuras 1a y 1b). Luego de eso, se ejecutó el modelo para las zonas cercanas al Puerto de Ilo, comparándose los resultados con los datos tomados en campo desde el ADCP con los del Modelo SMC y del modelo de desarrollo propio.

El modelo numérico desarrollado representa la hidrodinámica de olas y corrientes inducidas. Para ello emplea las ecuaciones fundamentales de movimiento, y de oleaje del tipo parabólico deducido en RefDif, que es un modelo bidimensional (x, y) a calado variable z, teniendo en cuenta el fenómeno de shoaling y refracción que sufren las olas al acercarse a la zona costera, desde un tiempo $t = 0$ hasta un tiempo final t, aplicado al puerto de Ilo. El punto de partida para el desarrollo de los diferentes módulos que conforman la simulación está dado por la recopilación de datos en la zona de interés, así como de fuentes globales. Esta información se detalla a continuación:

- Olas en aguas oceánicas proveniente de la NOAA (National Oceanographic and Atmospheric Administration) (Figura 2), las mismas que serán propagadas hacia aguas costeras cercanas al puerto de Ilo (Figuras 3 y 4). Esta información de oleaje de aguas profundas corresponde al nodo de Latitud 17.5 S y longitud 72.0 O, (Figura 5). Determinándose con la distribución estadística Log-Normal de 3 parámetros la altura significativa de diseño (Figura 6).
- Información batimétrica de detalle realizada por [21] ENAPU (2021) en el área de interés (Figura 4).
- Variables de calibración del modelo tales como: velocidad perturbada de aguas profundas, ángulo de aproximación de aguas profundas, coeficiente de rugosidad de Maning, y otros descritos en el apartado datos de calibración del presente trabajo de investigación.

A diferencia del presente modelo en Matlab, el modelo [6] SMC Mopla (2000) desarrollado por la Universidad de Cantabria presenta resultados en forma cualitativa y grafica. Este modelo ha sido ampliamente comprobado y es muy utilizado en estudios oceanográficos. Para realizar la simulación numérica con el software SMC, se necesitó adicionalmente tener la batimetría general de aguas profundas, desde la Carta Batimétrica General de los Océanos, GEBCO. (Figura 2).

Previamente y con ayuda de un programa Gis se procesa la información de la batimetría general que está en formato NetCDF desde el Gebco. Los resultados se obtienen en formato XYZ que se pueden visualizar con un software de curvas de nivel (Figura 3). Estos resultados son necesarios para el modelo SMC.

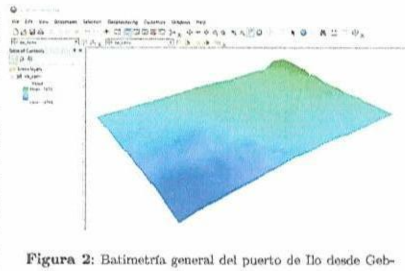

Figura 2: Batimetría general del puerto de Ilo desde Gebco.net

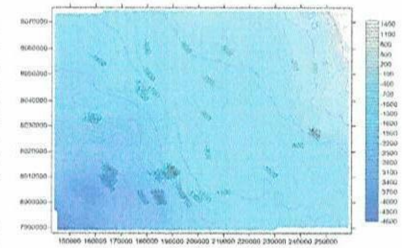

Figura 3: Curvas Topo-Batimétricas del puerto de Ilo en Surfer

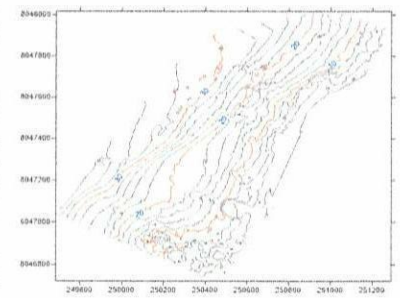

Figura 4: Batimetría de detalle para el puerto de Ilo en Surfer 8

Catorce - 14

Figura 5: Localización del nodo del modelo WW3 de la NOAA para datos de oleaje. *Extraído de [21] ENAPU PERÚ (2021).*

La variable de oleaje altura de ola Hs, proyectados desde data de la NOAA con la distribución log-Normal de 3 parámetros. Siendo el coeficiente de regresión obtenido de R^2=99.51 % para la altura de oleaje. El grafico representa la altura de ola significativa H_s con su respectiva probabilidad de excedencia. Para la presente simulación numérica se utilizó los datos de oleaje de 63 años. (Figura 6).

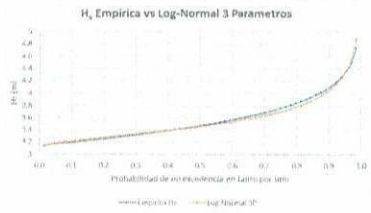

Figura 6: Proyección de la altura de Ola y período con tiempo de retorno en años.

TR	H_s
5	3.78844
10	4.05276
20	4.33978
50	4.76086
100	5.11470
200	5.50182
1000	6.54270

Tabla 1: Altura significativa (H_s) versus tiempo de retorno (TR)

La Tabla 1 muestra la altura significativa H_s probable con su respectivo período de retorno, dada la distribución de probabilidad Log-Normal de 3 parámetros.

Ecuaciones básicas de movimiento

Se utilizan las ecuaciones de Navier Stokes en coordenadas cartesianas con los ejes (x, y) dirigidos hacia el este y norte respectivamente y el eje z dirigido hacia arriba, siendo las componentes de la velocidad (u, v), [22] Periáñez (2010).

$$\frac{\partial u}{\partial t}+u\frac{\partial u}{\partial x}+v\frac{\partial u}{\partial y}=-f\times v-\frac{1}{\rho}\frac{\partial p}{\partial x}-\frac{\partial \Phi}{\partial x}+N_h\left(\frac{\partial^2 u}{\partial x^2}+\frac{\partial^2 u}{\partial y^2}\right)$$

$$\frac{\partial u}{\partial t}+u\frac{\partial u}{\partial x}+v\frac{\partial u}{\partial y}=-f\times u-\frac{1}{\rho}\frac{\partial p}{\partial y}-\frac{\partial \Phi}{\partial y}+N_h\left(\frac{\partial^2 v}{\partial x^2}+\frac{\partial^2 v}{\partial y^2}\right)$$

Las principales variables respecto al eje z fueron promediadas en este eje, por ello su variación respecto a z es despreciable. A continuación, se presenta la Tabla 2 con la descripción de las variables utilizadas.

Variable	Notación	Escala	Valor
Longitud	x, y	L	10^5
Profundidad	z	H	10^3
Velocidad Horizontal	u, v	U	10^{-1}
Velocidad Vertical	w	W	
Presión	p	P	10^7
Aceleración grav.	g	G	10
Parámetro de Coriolis	f	F	10^{-4}
Viscosidad molecular	μ	M	10^{-6}
Coef. Reynolds (x, y)	N_h, N_v	N_h, N_v	10^5
Coef. Reynolds (z)	N_z	N_z	10^{-1}
Densidad	ρ	ρ	10^3

Tabla 2: Escalas y ordenes de magnitud de las variables usadas. Los valores están en SI.

Discretización de las ecuaciones de movimiento

Con el fin de resolver numéricamente las ecuaciones de movimiento se desarrolló un algoritmo en diferencias finitas siendo el esquema de solución el de Upwind, [23] García et al. (2021). Este algoritmo es usado para ondas que intercambian su valor entre positivo y negativo de

sus principales variables de impulso [24] Guzmán (2020), obteniéndose:

$$\begin{aligned}
\frac{\partial u}{\partial t} &= \frac{u_{i,j}^{k+1}-u_{i,j}^{k}}{\Delta t}\\
u_p &= \left(\frac{u_{i,j}^{k}+\left|u_{i,j}^{k}\right|}{2}\right)\\
u_n &= \left(\frac{u_{i,j}^{k}-\left|u_{i,j}^{k}\right|}{2}\right)\\
ADVx &= u\frac{\partial u}{\partial x}+v\frac{\partial u}{\partial y}\\
&= +u_p\left\{\frac{u_{i,j}^{k}-u_{i-1,j}^{k}}{\Delta x}\right\}\\
&\quad +u_n\left\{\frac{u_{i+1,j}^{k}-u_{i,j}^{k}}{\Delta x}\right\}\\
GP_x &= g\left(\frac{\eta_{i,j}^{k}-\eta_{i-1,j}^{k}}{\Delta x}\right)\\
ROUx &= g\times e^2\times\frac{u_{i,j}^{k}\sqrt{\left(u_{i,j}^{k}\right)^2+\left(v_{i,j}^{k}\right)^2}}{\left(z_{i,j}\right)^{4/3}}\\
WSUxx &= \frac{Sxx_{i+1,j}-Sxx_{i,j}}{\rho_w\times\Delta x\times H_{i,j}^{k}}\\
WSUxy &= \frac{Sxy_{i,j+1}-Sxy_{i,j}}{\rho_w\times\Delta x\times H_{i,j}^{k}}\\
u_{i,j}^{k+1} &= u_{i,j}^{k}+\Delta t\,(-ADVx-GPx-ROU_x\\
&\qquad +WSUxx+WSUxy)
\end{aligned}$$

De manera similar se procede a discretizar el campo en el eje y, para el vector velocidad v.

$$\begin{aligned}
v_{i,j}^{k+1} &= v_{i,j}^{k}+\Delta t\,(-ADVy-GPy-ROU_y\\
&\qquad +WSUyy+WSUyx)
\end{aligned}$$

Ecuación de continuidad

Calculado el módulo de Navier Stokes se resuelve a continuación el módulo de conservación de masa, con el esquema FTBS (Forward Time-Backward Space) sobre el dominio de la zona en estudio. Luego se calcula la propagación del oleaje con el módulo Oluca [6] SMC (2000). El cual soluciona la ecuación parabólica de RefDif, obteniéndose finalmente el campo de corrientes.

$$\frac{\partial \eta}{\partial t}+\frac{\partial (u\times H)}{\partial x}+\frac{\partial (v\times H)}{\partial y}=0$$

$$\begin{aligned}
\frac{\partial \eta}{\partial t} &= \frac{\eta_{i,j}^{k+1}-\eta_{i,j}^{k}}{\Delta t}\\
DIVx &= \frac{\partial (u\times H)}{\partial x}\\
&= \left(\frac{u_{i+1,j}^{k}\times H_{i+1,j}^{k}-u_{i,j}^{k}\times H_{i,j}^{k}}{\Delta x}\right)\\
DIVy &= \frac{\partial (v\times H)}{\partial y}\\
&= \left(\frac{v_{i,j+1}^{k}\times H_{i,j+1}^{k}-u_{i,j}^{k}\times H_{i,j}^{k}}{\Delta y}\right)\\
\eta_{i,j}^{k+1} &= \eta_{i,j}^{k}-\Delta t\times(DIVx+DIVy)\\
H_{i,j}^{k+1} &= z_{i,j}+\eta_{i,j}^{k+1}
\end{aligned}$$

Descripción del modelo numérico SMC y sus principales parámetros

El Sistema de Modelado Costero (SMC) es una interfaz gráfica, la cual proporciona una herramienta computacional en el campo de la ingeniería de costas y Oceanografía. El modelo SMC resuelve el proceso de cálculo numérico que parte de datos de oleaje en aguas profundas, batimetría de detalle y general en aguas profundas. El módulo de propagación del oleaje Oluca incluye el shoaling, refracción y difracción, determinándose el campo de corrientes con ayuda de las ecuaciones de conservación de movimiento y masa. SMC (2000) [6].

Modelo de perturbación del oleaje Oluca-Q

El Grupo de Ingeniería Oceanográfica y de Costas (G.I.O.C.) desarrolló el modelo, Oluca-Q, el cual, a partir del campo de oleaje inicial obtiene los nuevos campos de oleaje, Méndez & Medina, (2005) [25].

Modelo de perturbación del tensor de radiación de corrientes de rotura

De forma paralela a como sucede con el oleaje [26] Barman & Paul (2016), las variaciones del fondo junto con las variaciones de altura de ola y dirección modifican las corrientes de rotura y el nivel medio, ya que el término forzador (tensor de radiación) es perturbado, Aragonés et al. (2017) [27].

Principales variables de calibración del modelo desarrollado

Entre los principales factores de calibración del modelo tenemos a la velocidad inicial perturbada U_o y V_o desde aguas profundas, el número de Courant CFL con el cual se determina el incremento de tiempo dt desde la ecuación de advección en cuanto a que el modelo halla la convergencia para CFL menores a 0.4, dx = 3.53 m, dy = 3.65 m, altura de oleaje de aguas profundas h_s de

Trece - 13

2.4 m, dirección de oleaje de 30.05° SSO, Giro y traslación de coordenadas de −30° con el fin de usar coordenadas cartesianas ortogonales y tener mayor dominio computacional (X, Y), el coeficiente de rugosidad de Maning es 0.02 para el cálculo de los esfuerzos cortantes Sxx, Syy y Sxy, el coeficiente de porosidad del lecho nporo siendo un valor promedio nporo= 0.32, la velocidad cuadrática media resultante $U_{rms} = 1.75$ m/s, el diámetro medio de las partículas del lecho marino $D_{50} = 0.28$ mm, el rango de amplitud de mareas y la influencia de la pendiente de fondo longitudinal y lateral por cuanto el modelo desarrollado converge para pendientes menores al cinco por mil.

Discusión de Resultados

Consideraciones Generales

Se observa la zona de batimetría realizada en torno al puerto girado 30° y la zona de dominio calculado a un $dx = 3.7840$ metros, $dy = 4.5232$ metros, $dt = 0.1374$ seg, el cual converge al sistema numérico para $CFL = 0.40$. El objetivo de girar la batimetría es la de tener mayor dominio computacional, dado que la discretización es en coordenadas cartesianas (x, y) (Figuras 7a y 7b)

Rosa de Oleaje

De los datos temporales de dirección y magnitud se obtiene que la dirección predominante es SSO, con una magnitud de 2.0 m a una probabilidad de ocurrencia del 24 % en el tiempo, y una altura de ola de 2.4 m a una probabilidad de ocurrencia del 14 % en promedio. Además, existe una magnitud pico de 3.0 m a una probabilidad de 8 % en el tiempo. (Figura 8)

Resultados de la Validación del Modelo

El modelo desarrollado en Matlab tiene buen coeficiente de correlación R2 igual a 89 % respecto a los datos tomados por el ADCP, y del 93 % entre los resultados del modelo SMC y los datos del ADCP. Siendo la media de velocidades de corrientes de los resultados en Matlab de 55.9 mm/s con desviación estándar relativa del 21.4 %, la velocidad promedio del SMC de 55.2 m/s con desviación estándar relativa de 29.1 %, y la velocidad promedio del ADCP es de 41.6 mm/s con desviación estándar relativa de 39 % (Tabla 3 y Figura 9).

La ventaja del modelo en Matlab a diferencia de los softwares de caja negra, es que se puede calibrar con gran número de variables descritas dentro del apartado 2.7, pudiéndose a su vez obtener resultados tanto numéricos como gráficos como se requiera al ser una sub-rutina editable. Lográndose con ello un mayor análisis al proyecto en estudio. Ambos modelos, el SMC y el desarrollado tienen similares resultados en corrientes. Ambos indican una fuerte concentración de vectores corriente al norte del puerto de ILO.

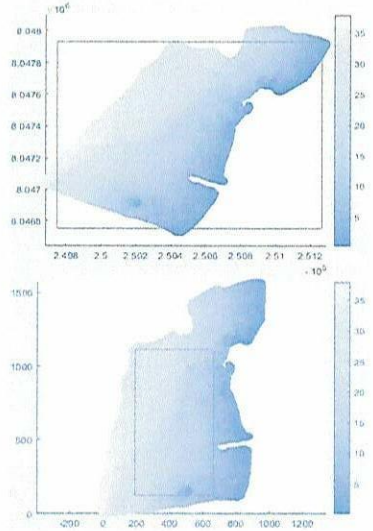

Figura 7: a) Batimetría detalle digital en Matlab del puerto de Ilo. b) Batimetría girada 30° en el sentido contrario al reloj.

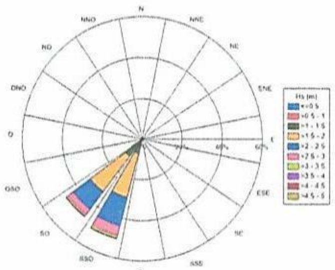

Figura 8: Rosa de oleaje de aguas profundas de la zona cercana al puerto de Ilo. *Extraído de ENAPU (2020)*

Validación ILO	
Versus	R2
Matlab-ADCP	89.21 %
SMC-ADCP	93.06 %

Tabla 3: Resultados de la Calibración del Modelo desarrollado versus SMC y el ADCP.

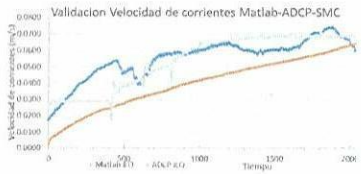

Figura 9: Resultados de la validación por velocidad de rrientes Matlab-ADCP-SMC.

Resultados de las corridas del programa mérico de corrientes y olas en Matlab

Se presentan los resultados de las corridas en el grama Matlab, observándose la evolución del oleaje y rrientes 2D para el dominio discretizado y girado 30° pecto al norte, con el fin de tener mayor dominio com tacional (Figuras 10a y 10b).

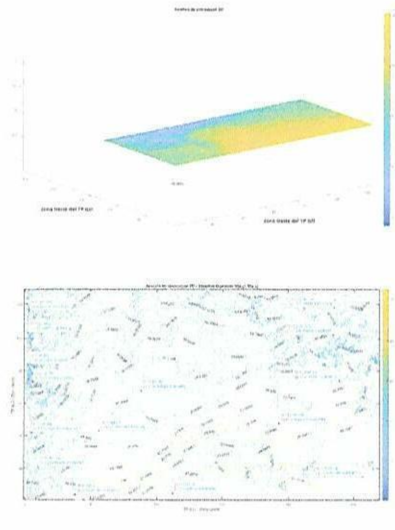

Figura 10: a) Análisis de circulación 2D (x, y) a calado variable z en Matlab. b) Corrientes 2D del puerto de Ilo en programa Matlab.

Resultados de la simulación numérica en SMC Mopla

De la Figura 11a, se observa una altura significativa de 1.30 metros en la ubicación del ADCP datos extraídos del estudio de ENAPU. Y de la Figura 11b se observa que existe una concentración de vectores corriente al Norte del puerto de Ilo, lo que podría conllevar a una mayor cantidad de sedimentos en esta zona.

De los resultados de la simulación numérica en Matlab se determinó que la concentración de corrientes es hacia la zona norte del puerto de Ilo (Figura 11b), y la simulación numérica en SMC se tiene una evolución similar hacia el norte del puerto (Figuras 11a y 11b).

Existe una similitud entre los datos tomados de campo con el ADCP y lo modelado con el SMC del 93 %, siendo la velocidad media del modelo de 55 mm/s y del ADCP de 41.6 mm/s, la velocidad media del modelo desarrollado es de 56 mm/s, las coordenadas del ADCP son: Este: 250268.7 y Norte: 8047305.5, Huso 19 del Perú.

Conclusiones

En este trabajo se determinó la hidrodinámica de corrientes y oleajes del Terminal Portuario (TP) de Ilo, se utilizaron tanto mediciones in situ de batimetría de detalle como modelos numéricos computacionales.

De la observación de los resultados de la rosa de oleaje proveniente de aguas profundas data de la NOAA por el modelo WW3 se determina que el oleaje predominante es de dirección SSO y SO hacia el norte en mayor probabilidad conllevándose a tener un flujo neto de corriente hacia el norte del puerto y erosión al sur de este, debido a la presencia del obstáculo natural de la península de Ilo.

Se recomienda que en futuros trabajos de investigación se realice el cálculo de velocidades de corriente utilizando los valores frecuenciales de distribución del oleaje en el tiempo, con la utilización de la rosa de oleaje. Así se podría obtener una proyección más acertada del cálculo de corrientes en el tiempo, proyectando, por ejemplo, tiempos desde 7200 segundos de corrida por cada probabilidad de oleaje (H altura y dirección Teta probables de oleaje en el delta de tiempo que transcurrió) hacia tiempos reales en un año. Esto daría una evolución más

Doce - 12

real proyectada de la posible variación hidrodinámica del TP en un año y compararlo con información tomada de campo con ADCP.

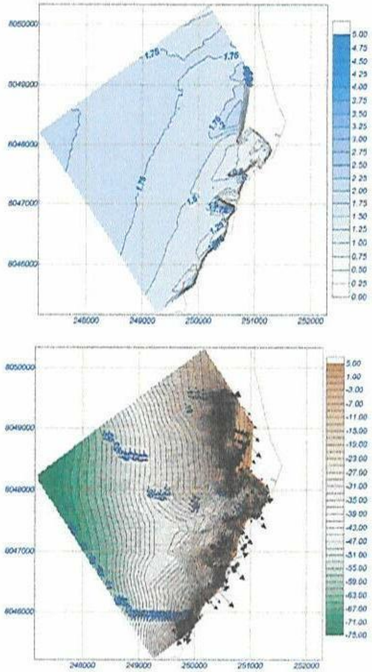

Figura 11: a) Gráfica SMC altura de ola significativa del TP ILO. b) Gráfico SMC de vectores corriente y batimetría del TP ILO.

Agradecimientos

Se hace referencia a la mayor voluntad de apoyo y disposición de la Empresa H&O Ingenieros Consultores S.A. y a la empresa nacional ENAPU quienes facilitaron información relevante en el desarrollo del presente estudio.

Apéndice (Simbología)

Cg = celeridad de grupo (m/s).

c = celeridad de la onda (m/s).

CFL = Número de Courant-Friedrichs-Levy.

$$CFL = \frac{\delta t}{\delta x / \sqrt{g \times h}}$$

dx, dy = Incremento en coordenadas cartesianas de los ejes x, y (m).

dt = Incremento de tiempo (s.)

E = Densidad de energía de ola (kg/s^2).

η = Elevación de la ola sobre el nivel de calado medio (m).

h = Calado en un punto del dominio (m).

δh = perturbación del fondo inducida por el transporte (m).

H = Altura total de ola (m).

δH = variación de altura de ola inducida por las variaciones del fondo (m).

θ = ángulo de la onda (°).

$\delta\theta$ = variación del ángulo inducida por las variaciones del fondo (°).

k = número de onda que cumple la relación de dispersión (m^{-1}).

σ = frecuencia angular de la onda (s^{-1}).

U, v = Velocidades de corrientes en los ejes x, y (m/s).

Sxx, Syy, Sxy = Esfuerzos cortantes en el lecho marino.

Referencias

[1] J. Kirby y R. Dalrymple. A parabolic equation for the combined refraction-diffraction of Stokes waves by mildly varying topography. Journal of Fluid Mechanics, **136**, 453-466, (1983). https://doi.org/10.1017/S0022112083002232

[2] J. Kirby y R. Dalrymple. Modelling waves in surfzones and around the islands. Journal of Waterway, Port, Coastal and Ocean Division, ASCE. **112** (1986). https://ascelibrary.org/doi/abs/10.1061/(ASCE)0733-950X(1986)112:1(78)

[3] APN. Autoridad Portuaria Nacional, *Plan Maestro del Terminal Portuario de Ilo* (2018), disponible en: https://webaplicacion.apn.gob.pe/proyecto/wp-content/uploads/2020/10/Plan-Maestro-Portuario-TP-ILO.pdf

[4] G. Solís, A. Guillén, A. Pilares, E. Saldaña, A. Werner. *Plan Estratégico del Terminal Portuario de Ilo, Tesis de Magister de Centrum PUCP*, (2011).

[5] B. Jigena, A. Arranz, A. Jigena, J. Monedero. Estudio del transporte marítimo y la explotación de la terminal de contenedores del Puerto de Cádiz (Study of the Maritime Transport and operation of Cádiz Port Container Terminal, Editorial Dykinson (Madrid), 1ra. Edición, **59**, (115) 1250-1274, ISBN: 978-84-1122-829-9, (2023). http://hdl.handle.net/10498/31756

[6] SMC. Universidad Cantabria. Sistema de modelado costero, Manual de usuario SMC 3.0, Modelo de oleaje, corrientes y evolución morfológica de una playa, Manual de referencia Eros 3.0, Modelo de erosión/sedimentación, Documento de referencia, volumen I, II, III, IV, V – Dinámicas, procesos litorales, obras, medio ambiente litoral, Apéndices, GIOC, UC, (2000).

[7] A. Mahmoodi, M. Lashteh, A. Mansouri, M. Shafai. Study of Current- and Wave-Induced Sediment Transport in the Nowshahr Port Entrance Channel by Using Numerical Modeling and Field Measurement, Journal of Marine Science and Engineering (2020), https://www.mdpi.com/2077-1312/8/4/284

[8] V. Leys y R. Mulligan. Modelling Coastal Sediment Transport for Harbour Planning: Selected Case Studies, CBCL Limited Consulting Engineers, Halifax NS 2East Carolina University, Greenville NC, (2015).

[9] A. Bennis, L. Furgerot, P. Bailly-Du Bois, F. Dumas, T. Odaka, C. Lathuilière, J. Filipot. Numerical modelling of three-dimensional wave-current interactions in complex environment: Application to Alderney Race. Appl. Ocean Res. **95**, (2020). http://dx.doi.org/10.1016/j.apor.2019.102021

[10] C. Calvino, T. Dabrowski & F. Dias. A study of the wave effects on the current circulation in galway bay, using the numerical model COAWST. Coastal Engineering (Amsterdam), **180**, (2023). https://doi.org/10.1016/j.coastaleng.2022.104251

[11] B. Jigena-Antelo, C. Estrada-Ludeña, S. Howden, W. Rey, J. Paz-Acosta, P. Lopez-García, E. Salazar-Rodriguez, N. Endrina, J. Muñoz-Pérez. Evidence of sea level rise at the Peruvian coast (1942–2019). Science of The Total Environment, **859**, Part 2, (2023b), https://doi.org/10.1016/j.scitotenv.2022.160082

[12] B. Jigena, J. Vidal and M. Berrocoso. Determination of the tide constituents at Livingston and Deception Islands (South Shetland Islands, Antarctica), using annual time series. **82**(191), 209-218, (2015). http://dx.doi.org/10.15446/dyna.v82n191.45207

[13] F. Ardhuin, A. Roland, F. Dumas, A. Bennis, A. Sentchev, P. Forget, J. Wolf, F. Girard, P. Osuna, M. Benoit. Numerical wave modeling in conditions with strong currents: Dissipation, refraction, and elative wind. J. Phys. Oceanogr. **42**(12), 2101–2120, (2012). http://dx.doi.org/10.1175/JPO-D-11-0220.1

[14] M. Olabarrieta, J. Warner, N. Kumar. Wave-current interaction in Willapa Bay. J. Geophys. Res.: Oceans **116**(C12), (2011). https://doi.org/10.1029/2011JC007387

[15] L. Renault, M. Molemaker, J. McWilliams, A. Shchepetkin, F. Lemarié, D. Chelton, S. Illig, A. Hall. Modulation of wind work by oceanic current interaction with the atmosphere. J. Phys. Oceanogr. **46** (6), 1685–1704, (2016). https://doi.org/10.1175/JPO-D-15-0232.1

[16] E. Guzmán. Modelamiento de corrientes superficiales inducidas por viento y marea en la bahía Ferrol-Chimbote, (2006). https://hdl.handle.net/20.500.12672/2535

[17] H. Varona y N. Alemán. Corrientes Marinas en el Tramo Costero Cazonal-Cazonalito". Ciencia en su PC, **IV**(4), (1999). https://hal.science/hal-04033150/document

Once - 11

Diez-10

[18] J. Muñoz-Perez, J. Gutierrez-Mas, J. Parrado, & L. Moreno. Sediment transport velocity by tracer experiment at Regla Beach (Spain). Journal of waterway port, coastal, and ocean engineering, **125**(6), 332-335, (1999). https://doi.org/10.1061/(ASCE)0733-950X(1999)125:6(332)

[19] G. Gómez-Pina, L. Fages, J. Ramírez, J. Muñoz-Pérez, & J. Enriquez. A critical review of beach restoration projects in the northern coast of Cadiz (Spain) after thirteen years. Coastal Engineering 2006: (5, 4167-4178, (2007). https://doi.org/10.1142/9789812709554_0350

[20] J. Muñoz-Pérez, I. Caballero, B. Tejedor, & G. Gomez-Pina. Reversal in longshore sediment transport without variations in wave power direction. Journal of Coastal Research, **26**(4), 780-786, (2010). https://doi.org/10.2112/08-1141.1

[21] ENAPU PERU. Estudio de pre inversión del proyecto a nivel perfil vinculado al mejoramiento de las facilidades portuarias en el terminal portuario de ilo, Informe Final: Estudio de oleaje, Estudio Meteorológico y Estudio de transporte de sedimentos, Elaborado por: Consorcio Puerto Ilo Incostas y H&O S.A. Código del documento: CPI-01-TS-IN-001, CPI-01-TP-IN-001 y CPI-01-OC-IN-003, (2021).

[22] R. Periáñez. *Fundamentos de Oceanografía Dinámica.* Universidad de Sevilla, España. ISBN 978-84-472-1235-4, (2010).

[23] P. García, A. Navas, J. Fernández. *Introducción a la Mecánica de Fluidos Computacional.* Prensas de la Universidad de Zaragoza, España ISBN 978-84-1340-233-8, (2021).

[24] E. Guzmán. Notas del curso Modelamiento de Sistemas Marítimos y Costeros, Lima-Perú, (2020).

[25] R. Méndez & P. Medina. A Perturbation Method for Wave and Wave-Induced Currents Computations in Beach Morphology Models, **77**, 393-402, (2005). https://ascelibrary.org/doi/abs/10.1061/40566(260)40

[26] N. Barman & A. Paul, *Coastal Morphodynamics Integrated Spatial Modeling on the Deltaic Balasore Coast*, India. **109**, ISBN 978-3-319-33574-2, (2016).

[27] L. Aragonés, I. López, E. Gómez-Martín, A. Jodá, S. García. *Ingeniería Marítima I*, Editorial Club Universitario, ISBN 9788416966479, España, (2017).

Nueve - 9

COB-2021-0929

COMPARISON OF THE THERMAL EFFICIENCY OF A GAS TURBINE WORKING WITH COMBUSTION AND DETONATION CHAMBERS

Ramiro Veronese de Vargas
Universidade Federal do Rio Grande do Sul, Rua Sarmento Leite, 425
ramiro_veronese@hotmail.com
Rodrigo Savi Justi
Universidade Federal do Rio Grande do Sul, Rua Sarmento Leite, 425
rodrigo.justi@ufrgs.br
César A. Quispe Gonzáles
Universidad Nacional Mayor de San Marcos, Lima District 15081, Peru
cquispeg@unmsm.edu.pe
Andrés A. Mendiburu Zevallos
Universidade Federal do Rio Grande do Sul, Rua Sarmento Leite, 425
International Research Group for Energy Sustainability (IRGES)
andresmendiburu@ufrgs.br

Abstract. The objective of the present study is to perform a thermodynamic comparison of the thermal efficiency by varying the main parameters of a power generation cycle involving gas turbines, where the combustion products are obtained in two different processes: by constant-pressure combustion inside a conventional combustion chamber and by a detonation process inside a detonation chamber. To achieve this goal, a study of combustion reactions in the context of equilibrium thermodynamics was performed; then, a computational model was developed in order to study the aforementioned processes. The thermodynamic model allows to study the influence of the compression ratio, fuel composition and equivalence ratio on the thermal efficiency and net-work generation.

The products composition was determined by applying the Gibbs-minimization method together with mass and energy conservation equations. On the other hand, the detonation temperature and the products composition after the detonation process were determined by applying the Chapman-Jouguet theory together with Gibbs-minimization, mass conservation and energy conservation equations. The results obtained show that the detonation-chamber-based turbine wields a higher thermal efficiency than the combustion-chamber-based turbine in all comparisons made utilizing equal initial parameters; however, the pressure and temperature of the chemical products in the detonation chamber are significantly higher, which, although theoretically beneficial, showcase practical limitations that imply the need of adaptations in the form of modifying the pre-and-post-combustion parameters and process in the thermodynamic energy generation process.

Keywords: *Detonation engine, combustion reaction, gas turbine, thermodynamic cycle*

1. INTRODUCTION

The gas turbines operating with combustion chambers at constant pressure are internal combustion engines extensively used in various fields of application, notably in the propulsion of aircraft, but also in the propulsion of ships and tanks and as electrical generators, pumps, and compressors (BORGNAKKE; SONNTAG, VAN WYLEN, 2002). Fuel combustion in gas turbines occurs in the combustion chamber. Turns (2011) develops a model where a combustion reaction occurs at constant pressure between air and fuel, resulting in combustion product gases.

Because they are so relevant in these fields, there is a high interest to improve the thermal efficiency of gas turbines; however, current conventional turbines have thermal efficiency very close to the theoretical ideal (LI *et al.*, 2018). Turbines operating with Rotating Detonation Engines (RDE) are an alternative technology to conventional turbines. In this type of turbine, the combustion chamber is a detonation chamber, where the speed of the products is supersonic. Reagents are fed through an annular cylindrical chamber and a detonation wave travels around the chamber in an helicoidal pattern. Continuous detonation is initiated only one time and operates at typical frequencies of 1-10Hz (BATTELLE, 2017). RDEs are a promising innovation because with them it is possible to obtain higher thermal efficiencies compared to turbines operating with conventional combustion chambers (WOLAŃSKI, 2017).

Naples and Hoke (2017) developed a rotating detonation engine and coupled the RDE with a T63 gas turbine. The RDE runs multiple power settings and demonstrates turbine performance equivalent to or better than the stock combustor using hydrogen fuel. Their results show that high frequency, 25% unsteady temporal pressure at a combustor outlet is not detrimental to uncooled turbine performance, and may even increase turbine efficiency. Numerical simulations were

performed by Yao *et al.* (2017) to RDEs with a hollow chamber, based on the reactive Euler equations and one-step Arrhenius chemistry model. The fuel injection area ratios range from 55.6% to 88.9% and the propulsive performance of the hollow RDE with different fuel injection area ratios is also evaluated and compared with experimental data and other simulation results.

Bigler *et al.* (2017) realized a comparative study between ideal thermodynamic cycles representing conventional gas turbines (using the Brayton cycle) and turbines with RDEs, using air as the working fluid; the detonation cycle presented a higher thermal efficiency as a function of all analyzed parameters. A comparation of the performance of a conventional Brayton cycle with a subsonic turbine and a detonation cycle with a supersonic turbine was realized by Sousa et al. (2017), through different compression ratios. The detonation cycle has a relative thermal efficiency gain of more than 6.7% for equal compression ratios.

Bluemner *et al.* (2019) performed an experimental study on the transition dynamics in a hydrogen-air rotating detonation combustors RDC as the operating mode transitions from two steadily propagating, equally-fast counter-rotating waves to a single wave depending on the operating condition. Their results indicate a correlation between the operating mode with two counter-rotating waves and choked flames, as well as quasi-detonations observed in generic detonation experiments in the literature. The work of Dai et al. (2019) develops a thermodynamic cycle where there is an extraction flow in the compressor, at 50% of the final pressure, which feeds the detonation chamber; the remaining air cools the product gases in a dilution process. A study about the effect of different K_2CO_3 ionized seed mass contents on the detonation process was realized by Lin *et al.* (2020). The PDE was successfully ignited and formed a stable detonation wave at ignition frequencies of 5 Hz and 10 Hz, and the peak pressure of the stable detonation with the ignition frequency of 5 Hz was 17% higher than that with an ignition frequency of 10 Hz.

The main objective of this work is to carry out a comparison between a thermodynamic cycle representing a conventional gas turbine, with a combustion chamber at constant pressure, and a thermodynamic cycle representing a turbine operating with an RDE, that is, with a detonation chamber. The parameters compared are the work supplied to the compressor, the work supplied by the turbine and principally the thermal efficiency of the cycle; these parameters are compared across a range of different compression ratios. Mathematical and computational models were developed to represent these two cycles operating in steady state and considering that the combustion and detonation processes reach equilibrium. The combustion products are mixed with air in a dilution process at constant pressure.

2. METHODOLOGY

The constant-pressure combustion thermodynamical cycle and the detonation cycle considered are shown, respectively, in the Figures 1 and 2. The cycles are compared across compression ratios, r, varying from 4 to 40. In the detonation cycle, air is extracted from the compressor in an intermediate pressure p_f; the ratio between p_f and the outlet pressure of the compressor p_1 is called the pressure fraction f. Three cases were considered for the detonation cycle, with values of f equal to 0,3, 0,5 and 0,7, respectively.

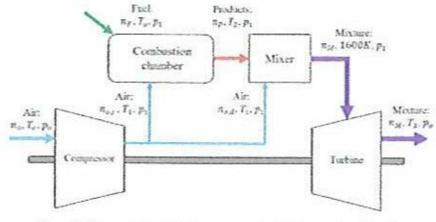

Figure 1. Scheme of the constant-pressure combustion thermodynamic cycle.

It is considered that the combustion is stoichiometric, being the reference pressure and temperature equal to 100.000 Pa and temperature 298,15 K, respectively (IUPAC, 1982). The global combustion reaction considered is shown in the Eq. (1).

$$C_{x_C}H_{x_H}O_{x_O}N_{x_N} + v_{ar}^{s}\,(O_2 + 3{,}76N_2) \rightarrow n_{CO_2}CO_2 + n_{CO}CO + n_{H_2O}H_2O + n_{H_2}H_2 + n_{O_2}O_2 + n_{N_2}N_2 \qquad (1)$$

Ocho - 8

where n_i is the mol number of the chemical species i, and ν_{ar}^{s} is the air coefficient of the reaction. The species in the products are H_2O, CO_2, N_2, O_2, H_2 and CO, the presence of H2 and CO denotes the possibility of incomplete combustion. The composition of the products is determined by applying the method of minimization of Gibbs free energy.

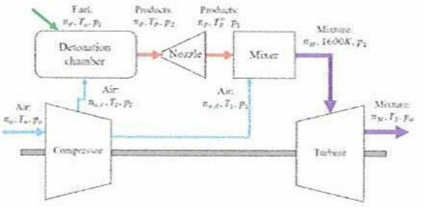

Figure 2. Scheme of the detonation thermodynamic cycle.

Considering the different equipment that form the cycle, the work done in the compressor W_C, in J, is determined by the Eq. (2).

$$W_C = n_o.(\bar{h}_i - \bar{h}_o) + n_{a,d}.(\bar{h}_1 - \bar{h}_i) \tag{1}$$

where n_o is total quantity of air which enters the compressor and $n_{a,d}$ is the quantity of air which goes to the mixer, called the dilution air, both in mol. $\bar{h}_o$, $\bar{h}_i$ and $\bar{h}_1$ are, respectively, the molar enthalpies of the air in the initial, intermediary and final states of the compression process, in J/mol; in the constant-pressure combustion cycle, there is no extraction air, so $\bar{h}_i = \bar{h}_1$. The molar enthalpies, as well as all other thermodynamical proprieties considered in this paper, are determined computationally utilizing the NASA-Glenn polynomials and coefficients (Gordon *et al.*, 2002). The air in the inlet is considered at the standard temperature and pressures of 293.15 K and 103 325 Pa and is composed of 21% of O_2 and 79% of N_2. n_o equals the sum of the quantity of dilution air $n_{a,d}$ with the quantity of reaction air $n_{a,r}$ [mol]. The quantity of reaction air is given by Eq. (3).

$$n_{a,r} = 4{,}76.\nu_{ar}^{s} \tag{3}$$

The isentropic efficiency η_C of the compressor is considered equal to 0,85. Equations (4) and (5) relate the isentropic efficiency with, respectively, the isentropic molar enthalpy of the intermediate state $\bar{h}_{is}$ and final state $\bar{h}_{1s}$ of the air and its real analogues, $\bar{h}_i$ and $\bar{h}_1$, and the molar enthalpy of the initial state $\bar{h}_o$, all in J/mol.

$$\eta_C = \frac{\bar{h}_{is} - \bar{h}_o}{\bar{h}_i - \bar{h}_o} \tag{4}$$

$$\eta_C = \frac{\bar{h}_{1s} - \bar{h}_o}{\bar{h}_1 - \bar{h}_o} \tag{5}$$

Equations (6) and (7) describe the isentropic compression processes from the initial state to the intermediary and final states, respectively.

$$\bar{s}_{1s}^{o} = \bar{s}_{o}^{o} + \bar{R}.\ln\frac{p_1}{p_o} \tag{6}$$

$$\bar{s}_{is}^{o} = \bar{s}_{o}^{o} + \bar{R}.\ln\frac{p_i}{p_o} \tag{7}$$

where $\bar{s}_o^o$, $\bar{s}_{is}^o$ and $\bar{s}_{1s}^o$ are, in this order, the molar entropies of the air in the initial state, in the intermediary isentropic state, and the final isentropic state, all in J/mol-K. $\bar{R}$ is the gas constant, equal to 8,134 J/mol-K. In the constant-pressure combustion chamber, the energy conservation is given by Eq. (8)

$$H_P = H_R \tag{8}$$

where H_P and H_R are, respectively, the total enthalpies of the products and the reactants, in J, given by the sum of the enthalpies of each of its component species. The products are at equilibrium, at an adiabatic flame temperature T_{ad}. In the detonation chamber the Chapman-Jouguet theory is applied, given by the system of equations shown in Eqs. (9) to (11).

$$\dot{m}'' = \rho_P.u_P = \rho_R.u_R \tag{9}$$

$$p_P + \rho_P.u_P^2 = p_R + \rho_R.u_R^2 \tag{10}$$

$$h_P + \frac{u_P^2}{2} = h_R + \frac{u_P^2}{2} \tag{11}$$

where $\dot{m}''$ is the mass flux, in kg/m²s; ρ_P and ρ_R are the specific masses of the products and reactants as a whole, in kg/m³; u_P and u_R are the velocities of the products and the reactants, in m/s; and h_P and h_R are the specific enthalpies of the products and reactants as a whole, in J/kg.

In the detonation cycle, the combustion products pass through a nozzle before entering the mixer, where their pressure is reduced from the detonation pressure until it equals the pressure of the dilution air. Equation (12) relates the stagnation temperature T_e, in K, with the temperature T, also in K, in an arbitrary point in the nozzle. k is the thermal capacity ratio and M is Mach number of the combustion products in this arbitrary point.

$$\frac{T}{T_e} = 1 + \frac{k-1}{2}M^2 \tag{12}$$

Equation (13) relates the stagnation pressure p_e, in Pa, with the pressure p, also in Pa, in an arbitrary point in the nozzle.

$$\frac{p}{p_e} = (1 + \frac{k-1}{2}M^2)^{\frac{k}{k-1}} \tag{13}$$

The product gases of the combustion go through the mixer where they are diluted with compressed air which got through the total compression process in the compressor. The temperature of the mixture of air and combustion products is considered equal to 1600 K, the upper limit of the range in which commercial turbines can safely operate (De Souza, 2014). The quantity of air needed to cool the product gases to 1600 K is given by the Eq. (14)

$$n_{a,d} = \frac{n_P(\bar{h}_{P,2} - \bar{h}_{P,1})}{(\bar{h}_{a,d,2} - \bar{h}_{a,d,1})} \tag{14}$$

where n_P is the quantity of the combustion products, in mol; $\bar{h}_{P,1}$ and $\bar{h}_{P,2}$ are the molar enthalpies of the product gases in the inlet and outlet of the mixer, respectively, in J/mol; and $\bar{h}_{a,d,1}$ and $\bar{h}_{a,d,2}$ are the molar enthalpies of dilution air in the inlet and outlet of the mixer, respectively, in J/mol. The air-products mixture enters the turbine, realizing an expansion work W_T, in J, given by the Eq. (15)

$$W_T = n_M.(\bar{h}_3 - \bar{h}_2) \tag{15}$$

where n_M is the quantity of mixture, in mol, and $\bar{h}_2$ and $\bar{h}_3$ are the molar enthalpies of the mixture in the inlet and outlet of the turbine, respectively, in J/mol. The isentropic efficiency η_T of the turbine is considered equal to 0,9. Equation (16) relates the isentropic efficiency with the isentropic molar enthalpy of the mixture in the outlet $\bar{h}_{3s}$ and its real analogue $\bar{h}_3$, as well as its inlet state $\bar{h}_2$, all in J/mol.

$$\eta_T = \frac{\bar{h}_2 - \bar{h}_3}{\bar{h}_2 - \bar{h}_{3s}} \tag{16}$$

Siete - 7

Equation (17) describes the isentropic expansion processes from the inlet state to the outlet state. The inlet pressure is equal to the outlet pressure of the compressor p_1. The outlet pressure is equal to the atmospheric pressure p_a.

$$\bar{s}^o_{3s} = \bar{s}^o_2 + \bar{R}.\ln\frac{p_1}{p_2} \tag{17}$$

The thermal efficiency of the cycle is given by Eq. (18).

$$\eta = \frac{W_T - W_C}{n_F.\overline{LHW}} \tag{18}$$

where n_F is the quantity of fuel, in mol, equal to 1. The molar lower heating value of the fuel, $\overline{LHW}$, is calculated via the Eq. (19)

$$\overline{LHW} = \frac{H_R - H_P}{n_F} = \sum_r^R n_r.\bar{h}^o_r - \sum_p^P n_p.\bar{h}^o_p \tag{19}$$

where the summations represent the sum of the molar enthalpies $\bar{h}^o_r$ and $\bar{h}^o_p$, in J/mol, of each component species of the reactants and products, respectively, in the reference state, multiplied by its respective quantity n_r or n_p, in mol. In this paper, the fuel considered is a synthesis gas obtained via gasification of biomass and residues (Babu, 2013). The composition of the synthesis gas is shown in Table 1.

Table 1. Composition of the fuel in mole fractions

Chemical species	Mole fraction
Carbon monoxide (CO)	0.48
Hydrogen (H_2)	0.32
Carbon dioxide (CO_2)	0.15
Nitrogen (N_2)	0.03
Methane (CH_4)	0.02

The synthesis gas yields a $\overline{LHW}$ of 229 284.78 J/mol and has a molar formation enthalpy at the reference state $\bar{h}^o_F$ of -113 568.72 J/mol. The air coefficient ν^t_{ar} is equal to 0.44 and the quantity of reaction air $n_{a,r}$ is equal to 2.0944 mol.

3. RESULTS AND DISCUSSIONS

The results obtained using the computational models, pertaining to the thermal efficiency and the total work to the compressor and from the turbine, in each case, are presented and commented in the following sub-sections.

3.1. Work done in the compressor

The work needed by the compressor is similar between the three analyzed cases of the detonation cycle, as shown in the Figure 3. For the same compression ratio, the larger the pressure fraction, the larger is the fraction of the total work needed for the compression of the reaction air; although, due the lower temperature of the combustion products at the outlet of the nozzle (as shown in the Table 2), this effect is compensated by the smaller quantity of dilution air needed to cool the product gases to 1600 K.

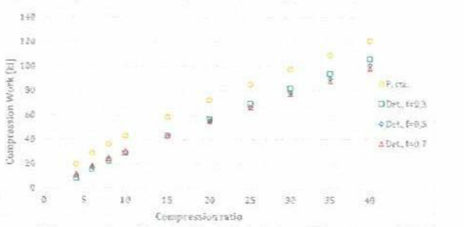

Figure 3. Work done in the compressor for constant-pressure combustion cycle (P.cte) and detonation cycle for three different pressure fractions ($f = 0{,}3$, $f = 0{,}5$ and $f = 0{,}7$) as a function of the compression ratio

Table 2. Inlet turbine temperature [K]; for the constant-pressure combustion, equal to the adiabatic flame temperature; for the detonation, equal to the outlet nozzle temperature.

r	4	6	8	10	15	20	25	30	35	40
p = const.	2202.2	2237.8	2265.4	2288.3	2333.1	2367.0	2396.3	2420.8	2442.4	2461.7
f = 0.3	2059.2	2129.4	2180.7	2221.4	2297.4	2353.2	2397.6	2434.7	2466.5	2494.6
f = 0.5	1952.7	2019.6	2068.6	2107.5	2180.3	2234	2276.7	2312.7	2343.2	2370.3
f = 0.7	1886.0	1950.8	1998.4	2036.3	2107.3	2159.5	2201.3	2236.2	2266.3	2292.9

The work done in the compressor in the constant-pressure combustion cycle is significantly larger in comparison with the detonation cycle. That occurs for two reasons: first, for an equal compression ratio r, all the air that enters the compressor in the constant-pressure cycle is compressed at this ratio, in contrast with the detonation cycle, where only the dilution air is compressed at r, with the rest being compressed just at r_f; second, the inlet temperatures of the combustion products in the mixer are larger in the constant-pressure cycle because there was no nozzle considered in that case.

3.2. Work done by the turbine

The inlet temperature and pressure and the outlet pressure in the turbine are always the same in all the considered scenarios; the only variable parameters, that influence the enthalpy difference between the outlet and inlet of the turbine, are the quantity and composition of the product gases, the quantity of dilution air and the outlet temperature of the air-products mixture.

The fraction of the total work performed by the expansion of the combustion gases is a negligible factor in the case-by-case comparison, due to its quantity and composition being approximately the same in all cases studied in the present work. The outlet temperature of the mixture is also a negligible factor in the analysis. The turbine outlet temperature is shown in the Table 3 for different compression ratios and intermediate pressures.

Table 3. Outlet turbine temperature [K].

r	4	6	8	10	15	20	25	30	35	40
p = const.	1225.2	1132.3	1070.1	1023.8	944.0	890.6	850.9	819.6	793.8	772.1
f = 0.3	1226.3	1132.7	1069.9	1023.2	942.6	888.6	848.6	817.1	791.2	769.4
f = 0.5	1229.3	1136.1	1073.5	1026.8	946.2	892.2	852.1	820.5	794.5	772.6
f = 0.7	1231.5	1138.5	1076.0	1029.4	948.8	894.7	854.6	822.8	796.8	774.8

Seis-6

It is observed that for larger pressure fractions in the detonation cycle, the outlet temperature in the outlet of nozzle is lower. Therefore, a smaller quantity of dilution air is needed for the cooling process, consequently, diminishing the work done by the turbine. The turbine work in the detonation cycle in most cases is smaller than the turbine work in the constant-pressure cycle, as shown in the Figure 4, except for $f = 0.3$. In that case, the work is larger for compression ratios larger than 25, the inlet temperature in the mixer surpasses its equivalent in the constant-pressure cycle, being need a larger quantity of dilution air.

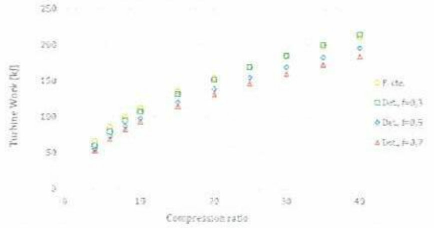

Figure 4. Work done by the turbine for constant-pressure combustion cycle (P.cte) and detonation cycle for three different pressure fractions ($f = 0{,}3$, $f = 0{,}5$ and $f = 0{,}7$) as a function of the compression ratio.

3.3. Thermal efficiency

The thermal efficiency curves of the three analyzed detonation cycles behave similarly when compared with each other. However, the largest thermal efficiency was obtained for the case of the pressure fraction equal to 0,3, as shown in the Figure 5. The Figure also contains the thermal efficiency of cycle gas turbines of fabricant Mitsubishi Hitachi Power Systems, tested with natural gas for different pressure ratios. These values can be compared with the thermal efficiency of constant-pressure combustion cycle calculated by the developed model. The specifications of these gas turbines can be founded in Table 4. Was not found data for detonation cycles with similar operating conditions to those studied in this work. It can be observed that for compressions ratios between 14 and 23 the experimental thermal efficiency of Mitsubishi Hitachi Gas Turbines falls between 34.9 and 41.0 %, this is in accordance with the results obtained with the model developed in the present work, which determined thermal efficiencies among 33.9 and 35.9% for compression ratios between 20 and 25. The difference in thermal efficiencies can be explained by higher concentration of inert gases in the syngas used for the simulations performed in this work.

Table 4. Thermal efficiencies of simple cycle gas turbines of fabricant Mitsubishi Hitachi Power Systems tested with natural gas (Gas Turbine World, 2014).

Model	Power (MW)	Mass flow rate (kg/s)	Compression Ratio	Thermal Efficiency (%)	Heat rate (kJ/kWh)
M501DA	113.9	346.1	14.0	34.9	10318.4
M501F3	185.4	458.6	16.0	37.0	9738.1
H-80	110.6	307.2	19.2	37.6	9584.1
M501G1	267.5	598.8	20.0	39.1	9210.7
M501J	327.0	598.8	23.0	41.0	8783.3

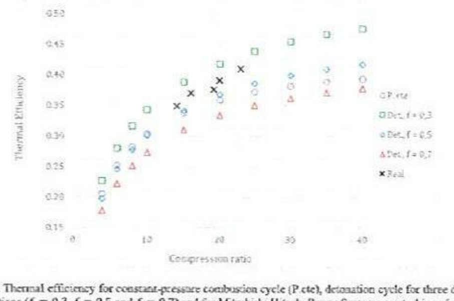

Figure 5. Thermal efficiency for constant-pressure combustion cycle (P.cte), detonation cycle for three different pressure fractions ($f = 0{,}3$, $f = 0{,}5$ and $f = 0{,}7$) and for Mitsubishi Hitachi Power Systems gas turbines (real) as a function of the compression ratio.

When compared to the constant-pressure combustion cycle, only the detonation cycle at $f = 0.3$ possesses a larger thermal efficiency for all the values of r considered in the analysis. At $f = 0.5$, the thermal efficiency surpasses the constant-pressure cycle only for compression ratios larger than 10, approximately. The thermal efficiency of the detonation cycle at $f = 0.7$ is smaller than the constant-pressure cycle for all pressure ratios considered. Table 5 shows the relative gains of the detonation cycles in comparison with the constant-pressure combustion cycle.

The thermal efficiency curves of the detonation cycles grow faster, with the increase of r, than the curve of the constant-pressure cycle. Therefore, it is possible to infer that the termal efficiency of the detonation cycle at $f = 0.7$ outgrows the constant-pressure cycle for compression ratios larger than 40; only further simulations can confirm this hypothesis, tough. However, the fact that a lower compression, $f = 0.3$, is enough to surpass the efficiency of the constant-pressure cycle is an important result which shows the advantage of the detonation cycle, since there is an increase in pressure inside the detonation chamber.

Table 5. Relative gains in thermal efficiency of the detonation cycles compared to the constant-pressure combustion cycle.

r	4	6	8	10	15	20	25	30	35	40
$f = 0.3$	10.63%	11.09%	12.00%	12.90%	14.87%	16.46%	17.79%	18.94%	19.96%	20.90%
$f = 0.5$	-3.55%	-2.60%	-1.59%	-0.70%	1.10%	2.48%	3.59%	4.56%	5.36%	6.11%
$f = 0.7$	-13.29%	-11.95%	-10.85%	-9.95%	-8.24%	-7.01%	-6.04%	-5.23%	-4.55%	-3.94%

Due to the detonation cycle using a supersonic turbine, the kinetic energy variation can be a significant component in the energy balance of the turbine. In future works, the kinetic energy variation should be considered, with a dynamic analysis of the turbine being needed; this is beyond the scope of the present work. It can be inferred, although, that the thermal efficiency of the detonation cycle should be higher for every pressure fraction f if the kinetic energy variation was considered.

4. CONCLUSIONS

The comparison between the results obtained with the thermodynamic models for the gas turbine working with a constant-pressure combustion chamber and with a detonation combustion chamber, shows the increase of the thermal efficiency for low extraction pressure ratios (f=0.3). In general, the thermal efficiency of the detonation cycle decreases with increasing extraction pressure ratios.

The constant-pressure cycle presents a higher compression work than the detonation cycle. However, the work performed by the turbine, for the constant-pressure cycle, is slightly higher than that performed with the detonation cycle.

Cinco – 5

The work performed by the turbine increases as the extraction pressure ratio is lower ($f=0.3$). In the case of $f=0.3$, the relative gain in thermal efficiency increases with the compression ratio from 10.63% at $r=4$ to 20.90% for $r=40$.

In future works, the strategy for lowering the temperature of the products leaving the detonation chamber can also be considered as a variable parameter. It is also possible to show the variation of the thermal efficiency by changing the turbine inlet temperature, which was considered constant, and equal to 1600K in the present work. Future work can also consider more complex cycle in order to obtain further increases in the thermal efficiency.

5. REFERENCES

Basu, Prabir, and Biomass Gasification, 2017. "Pyrolysis and Torrefaction Practical Design and Theory." (2013).

Naples, Andrew, et al. "RDE implementation into an open-loop T63 gas turbine engine." *55th AIAA Aerospace Sciences Meeting.*

Bigler, Blaine R., Eric J. Paulson, and William A. Hargus, 2017. "Idealized efficiency calculations for rotating detonation engine rocket applications." *53rd AIAA/SAE/ASEE Joint Propulsion Conference.*

Bluemner, R., et al, 2019. "Counter-rotating wave mode transition dynamics in an RDC." *International Journal of Hydrogen Energy* 44.14: 7628-7641.

Borgnakke, C.; Sonntag, R.E.; Van Wylen, G. J., 2002. "Fundamentos da Termodinâmica: Tradução da 5ª edição americana". *São Paulo: Edgard Blücher.*

CARVALHO JR., J. A. et al., 2018. "Combustão aplicada". 1. ed. *Florianópolis: EdUFSC.*

Shapiro, Howard N., and Michael J. Moran, 2009. "Princípios de termodinâmica para engenharia." *LTC,* Ed 6.

Qi, Lei, et al., 2019. "Investigation of the pressure gain characteristics and cycle performance in gas turbines based on interstage bleeding rotating detonation combustion." *Entropy* 21.3: 265.

DAI, Y. et al., 2019. "Investigation of the Pressure Gain Characteristics and Cycle Performance in Gas Turbines Based on Interstage Bleeding Detonation Combustion." *Applied Mechanics and Materials, [s. l.], v. 782, p. 3–12.*

De Souza, Z., 2014 "Plantas de Geração Térmica a Gás: Turbina a Gás, Turbocompressor, Recuperador de Calor, Câmara de Combustão." *1. ed. Rio de Janeiro: Interciência.*

Fox, Robert W., Philip J. Pritchard, and Alan T. McDonald, 2000. "Introdução à Mecânica Dos Fluidos". *Grupo Gen-LTC.*

Gas Turbine World, 2014 Performance Specs, *Vol. 44, No. 1, January–February 2014, Pequot Publis- hing, 2014.*

Gordon, S.; McBride, B. J.; Zehe, M. J., 2002. "NASA Glenn Coefficients for Calculating Thermodynamic Properties of Individual Species." *Washington D.C.: NASA.*

IUPAC, 1982. "Notation for states and processes, significance of the word standard in chemical thermodynamics, and remarks on commonly tabulated forms of thermodynamic functions." *Pure & Applied Chemistry, [s. l.], v. 54, n. 6, p. 1239–1250.*

LEE, J. H. S., 2008. "The Detonation Phenomenon." *1. ed. Cambridge: Cambridge University Press.*

Li, Z. et al., 2018. "A Thermodynamic Analysis of the Pressure Gain of Continuously Rotating Detonation Combustor for Gas Turbine." *Applied Sciences, [s. l.], v. 8, n. 4, p. 535–553.*

Lin, Ling, et al., 2020. "Experimental study on the detonation process of a pulse detonation engine with ionized seeds." *Defence Technology* 16 :178-187.

Sousa, Jorge, Guillermo Paniagua, and Elena Collado Morata, 2017. "Thermodynamic analysis of a gas turbine engine with a rotating detonation combustor." *Applied energy* 195: 247-256.

Morata, Elena C.; Paniagua, Guillermo; Sousa, Jorge, 2017. "Thermodynamic analysis of a gas turbine engine with a rotating detonation combustor." *Applied Energy, [s. l.], v. 195, p. 247–256.*

NIST. JANAF, 1971. "Thermochemical Tables. 2. ed. *Gaithersburg: National Bureau of Standards.*

Saad, M. A, 1992. "Compressible Fluid Flow." *2. ed. Hoboken: Prentice Hall.*

Turns, S, 2012. "An Introduction to Combustion: Concepts and Applications." 3. ed. *New York: McGraw-Hill.*

Wolański, Piotr, 2015. "Application of the continuous rotating detonation to gas turbine." *Applied Mechanics and Materials.* Vol. 782. Trans Tech Publications Ltd.

Yao, Songbai, et al, 2017. "Numerical study of hollow rotating detonation engine with different fuel injection area ratios." *Proceedings of the Combustion Institute* 36.2:2649-2655.

6. RESPONSIBILITY NOTICE

The author(s) is (are) the only responsible for the printed material included in this paper.

Cuatro-4

SOLICITO LICENCIA AL CARGO DE DIRECTOR(e) DEL DEPARTAMENTO ACADÉMICO DE INGENIERÍA MECÁNICA DE FLUIDOS POR ELECCIONES

SEÑOR DECANO DE LA FACULTAD DE CIENCIAS FÍSICAS
Dr. ÁNGEL BUSTAMANTE DOMINGUEZ

CÉSAR ALEJANDRO QUISPE GONZALES, identificado con DNI N° 10394420, docente Principal Tiempo Completo 40 horas, del Departamento Académico de Ingeniería Mecánica de Fluidos, con código docente N° 084492, ante su despacho me presento y expongo:

Que habiéndose convocado el proceso de elecciones de Decanos de Facultades a nivel de la Universidad Nacional Mayor de San Marcos (Proceso 2025), al cual voy a presentarme como candidato, y siendo requisito indispensable que los candidatos no ostenten cargo en su facultad, debiendo solicitar la licencia respectiva al cargo que ocupan:

SOLICITO:

Se me otorgue una licencia temporal, a partir de la fecha 03 de abril de 2025 y mientras dure el proceso de elecciones, al cargo de Director del Departamento de Ingeniería Mecánica de Fluidos, que me fue encargado por su Despacho mediante Resolución Rectoral N° 013954-2024-R/UNMSM de fecha 22 de noviembre de 2024, lo que me permitirá cumplir con los requisitos dispuestos por el Comité Electoral, para las próximas elecciones que se avecinan.

POR LO EXPUESTO:

A Ud. solicito Sr. Decano, acceder a mi solicitud por ser de justicia.

C. U. 03 de abril de 2025

César Alejandro Quispe Gonzales
DNI 10394420
Cód. UNMSM 084492

Tres - 3

UNMSM

Firmado digitalmente por TELLO PIRETA Rosa Ines FAU 20148092282 soft
Motivo: Soy el autor del documento
Fecha: 03.04.2025 14:24:56 -05:00

MESA DE PARTES - MP - FCF

HOJA DE ENVÍO N° 000514-2025-MP-DA-FCF/UNMSM

FECHA
03/04/2025

EXPEDIENTE : **UNMSM-20250042721**

ASUNTO: QUISPE GONZALES CÉSAR ALEJANDRO -SOLICITO LICENCIA AL CARGO DE DIRECTOR (e) DEL DEPARTAMENTO ACADEMICO DE INGENIERIA MECANICA DE FLUIDOS POR ELECCIONES - INGRESO DE DOCUMENTOS - FCF - COD: 084492 - DOC: 10394420 - AP. PAT.: QUISPE

REFERENCIA : FUT VIRTUAL Nº 00699653 INGRESO DE DOCUMENTOS - FCF - COD: 084492 - DOC: 10394420 - AP. PAT.: QUISPE

DEPENDENCIA DESTINO	TRAMITE	PRIORIDAD	INDICACIONES
DECANATO - D - FCF	ORIGINAL	NORMAL	

TELLO PIRETA ROSA INES

JEFE DE UNIDAD

Dos - 2

SOLICITO LICENCIA AL CARGO DE MIEMBRO DEL CONSEJO DE FACULTAD DE CIENCIAS FÍSICAS POR ELECCIONES

SEÑOR DECANO DE LA FACULTAD DE CIENCIAS FÍSICAS
Dr. ÁNGEL BUSTAMANTE DOMINGUEZ

CÉSAR ALEJANDRO QUISPE GONZALES, identificado con DNI N° 10394420, docente Principal Tiempo Completo 40 horas, del Departamento Académico de Ingeniería Mecánica de Fluidos, con código docente N° 084492, ante su despacho me presento y expongo:

Que habiéndose convocado el proceso de elecciones de Decanos de Facultades a nivel de la Universidad Nacional Mayor de San Marcos (Proceso 2025), al cual voy a presentarme como candidato, y siendo requisito indispensable que los candidatos no ostenten cargo en su facultad, debiendo solicitar la licencia respectiva al cargo que ocupan:

SOLICITO:

Se me otorgue una licencia temporal, a partir de la fecha 03 de abril de 2025 y mientras dure el proceso de elecciones, al cargo de Miembro del Consejo de Facultad de Ciencias Físicas, que actualmente ocupo; lo que me permitirá cumplir con los requisitos dispuestos por el Comité Electoral, para las próximas elecciones que se avecinan.

POR LO EXPUESTO:

A Ud. solicito Sr. Decano, acceder a mi solicitud por ser de justicia.

C. U. 03 de abril de 2025

César Quispe G

César Alejandro Quispe Gonzales
DNI 10394420
Cód. UNMSM 084492

Uno - 1

UNMSM Firmado digitalmente por TELLO PIRETA Rosa Ines FAU 20148092282 soft
Motivo: Soy el autor del documento
Fecha: 03.04.2025 15:42:34 -05:00

MESA DE PARTES - MP - FCF

HOJA DE ENVÍO N° 000516-2025-MP-DA-FCF/UNMSM

FECHA
03/04/2025

EXPEDIENTE : **UNMSM-20250042803**

ASUNTO: QUISPE GONZALES CÉSAR ALEJANDRO - SOLICITO LICENCIA AL CARGO DE MIEMBRO DEL CONSEJO DE FACULTAD DE CIENCIAS FISICAS POR ELECCIONES - INGRESO DE DOCUMENTOS - FCF - COD: 084492 - DOC: 10394420 - AP. PAT.: QUISPE

REFERENCIA : FUT VIRTUAL Nº 00699727 INGRESO DE DOCUMENTOS - FCF - COD: 084492 - DOC: 10394420 - AP. PAT.: QUISPE

DEPENDENCIA DESTINO	TRAMITE	PRIORIDAD	INDICACIONES
DECANATO - D - FCF	ORIGINAL	NORMAL	

TELLO PIRETA ROSA INES

JEFE DE UNIDAD